



HAL
open science

Jovian Temperature and Cloud Variability during the 2009-2010 Fade of the South Equatorial Belt

Leigh N. Fletcher, G.S. Orton, J.H. Rogers, A.A. Simon-Miller, I. de Pater,
M.H. Wong, O. Mousis, P.G.J. Irwin, M. Jacquesson, P.A. Yanamandra-Fisher

► **To cite this version:**

Leigh N. Fletcher, G.S. Orton, J.H. Rogers, A.A. Simon-Miller, I. de Pater, et al.. Jovian Temperature and Cloud Variability during the 2009-2010 Fade of the South Equatorial Belt. *Icarus*, 2011, 10.1016/j.icarus.2011.03.007 . hal-00756915

HAL Id: hal-00756915

<https://hal.science/hal-00756915>

Submitted on 24 Nov 2012

HAL is a multi-disciplinary open access archive for the deposit and dissemination of scientific research documents, whether they are published or not. The documents may come from teaching and research institutions in France or abroad, or from public or private research centers.

L'archive ouverte pluridisciplinaire **HAL**, est destinée au dépôt et à la diffusion de documents scientifiques de niveau recherche, publiés ou non, émanant des établissements d'enseignement et de recherche français ou étrangers, des laboratoires publics ou privés.

Accepted Manuscript

Jovian Temperature and Cloud Variability during the 2009-2010 Fade of the South Equatorial Belt

Leigh N. Fletcher, G.S. Orton, J.H. Rogers, A.A. Simon-Miller, I. de Pater, M.H. Wong, O. Mousis, P.G.J. Irwin, M. Jacquesson, P.A. Yanamandra-Fisher

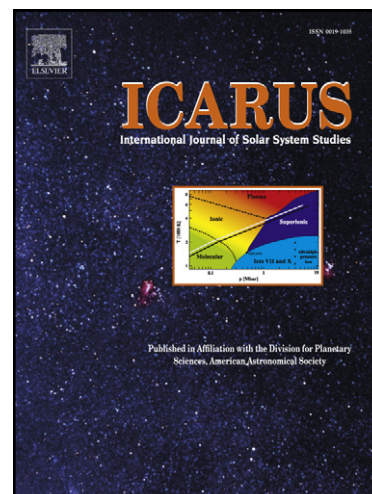
PII: S0019-1035(11)00091-1
DOI: [10.1016/j.icarus.2011.03.007](https://doi.org/10.1016/j.icarus.2011.03.007)
Reference: YICAR 9750

To appear in: *Icarus*

Received Date: 29 October 2010
Revised Date: 10 March 2011
Accepted Date: 11 March 2011

Please cite this article as: Fletcher, L.N., Orton, G.S., Rogers, J.H., Simon-Miller, A.A., de Pater, I., Wong, M.H., Mousis, O., Irwin, P.G.J., Jacquesson, M., Yanamandra-Fisher, P.A., Jovian Temperature and Cloud Variability during the 2009-2010 Fade of the South Equatorial Belt, *Icarus* (2011), doi: [10.1016/j.icarus.2011.03.007](https://doi.org/10.1016/j.icarus.2011.03.007)

This is a PDF file of an unedited manuscript that has been accepted for publication. As a service to our customers we are providing this early version of the manuscript. The manuscript will undergo copyediting, typesetting, and review of the resulting proof before it is published in its final form. Please note that during the production process errors may be discovered which could affect the content, and all legal disclaimers that apply to the journal pertain.



Jovian Temperature and Cloud Variability during the 2009-2010 Fade of the South Equatorial Belt

Leigh N. Fletcher^a, G.S. Orton^b, J.H. Rogers^c, A. A. Simon-Miller^d, I. de Pater^e,
M.H. Wong^e, O. Mousis^f, P.G.J. Irwin^a, M. Jacquesson^g, P.A.
Yanamandra-Fisher^b

^a*Atmospheric, Oceanic & Planetary Physics, Department of Physics, University of Oxford,
Clarendon Laboratory, Parks Road, Oxford, OX1 3PU, UK*

^b*Jet Propulsion Laboratory, California Institute of Technology, 4800 Oak Grove Drive,
Pasadena, CA, 91109, USA*

^c*British Astronomical Association, Burlington House, Piccadilly, London W1J 0DU, UK*

^d*NASA/Goddard Spaceflight Center, Greenbelt, Maryland, 20771, USA*

^e*University of California, Berkeley, Astronomy Dept., 601 Campbell Hall, Berkeley, CA
94720-3411, USA*

^f*Institut UTINAM, CNRS-UMR 6213, Observatoire de Besançon, Université de Franche-Comté,
Besançon, France*

^g*JUPOS Team, C/O British Astronomical Association, Burlington House, Piccadilly, London W1J
ODU, UK.*

Abstract

Mid-infrared 7-20 μm imaging of Jupiter from ESO's Very Large Telescope (VLT/VISIR) demonstrate that the increased albedo of Jupiter's South Equatorial Belt (SEB) during the 'fade' (whitening) event of 2009-2010 was correlated with changes to atmospheric temperature and aerosol opacity. The opacity of the tropospheric condensation cloud deck at pressures less than 800 mbar increased by 80% between May 2008 and July 2010, making the SEB (7-17°S) as opaque in the thermal infrared as the adjacent equatorial zone. After the cessation of discrete convective activity within the SEB in May 2009, a cool band of high aerosol opacity (the SEB zone at 11-15°S) was observed separating the cloud-free north-

Email address: fletcher@atm.ox.ac.uk (Leigh N. Fletcher)

ern and southern SEB components. The cooling of the SEBZ (with peak-to-peak contrasts of 1.0 ± 0.5 K), as well as the increased aerosol opacity at 4.8 and 8.6 μm , preceded the visible whitening of the belt by several months. A chain of five warm, cloud-free ‘brown barges’ (subsiding airmasses) were observed regularly in the SEB between June 2009 and June 2010, by which time they too had been obscured by the enhanced aerosol opacity of the SEB, although the underlying warm circulation was still present in July 2010. Upper tropospheric temperatures (150-300 mbar) remained largely unchanged during the fade, but the cool SEBZ formation was detected at deeper levels ($p > 300$ mbar) within the convectively unstable region of the troposphere. The SEBZ formation caused the meridional temperature gradient of the SEB to decrease between 2008 and 2010, reducing the vertical thermal windshear on the zonal jets bounding the SEB. The southern SEB had fully faded by July 2010 and was characterised by short-wave undulations at 19-20°S. The northern SEB persisted as a narrow grey lane of cloud-free conditions throughout the fade process.

The cool temperatures and enhanced aerosol opacity of the SEBZ after July 2009 are consistent with an upward flux of volatiles (e.g., ammonia-laden air) and enhanced condensation, obscuring the blue-absorbing chromophore and whitening the SEB by April 2010. These changes occurred within cloud decks in the convective troposphere, and not in the radiatively-controlled upper troposphere. NH_3 ice coatings on aerosols at $p < 800$ mbar are plausible sources of the suppressed 4.8 and 8.6- μm emission, although differences in the spatial distribution of opacity at these two wavelengths suggest that enhanced attenuation by a deeper cloud ($p > 800$ mbar) also occurred during the fade. Revival of the dark SEB coloration in the coming months will ultimately require sublimation of these ices

by subsidence and warming of volatile-depleted air.

Keywords: Jupiter, Atmospheres, composition, Atmospheres, structure

1 **1. Introduction**

2 Jupiter's axisymmetric structure, consisting of bright zones and dark brown
3 belts, can undergo dramatic visible changes over short time scales. The most
4 impressive of these is the variability of the South Equatorial Belt (SEB, 7-17°S),
5 which can change from the broadest and darkest belt on the planet to a white
6 zone-like appearance over a matter of months. The SEB, which lies in Jupiter's
7 southern tropics and contains the Great Red Spot (GRS) at its southern edge, is
8 typically a dark brown stripe encircling the globe between two opposing zonal
9 flows (Fig. 1a): a prograde (eastward) jet at 7°S and the planet's fastest retrograde
10 (westward) jet at 17°S (all latitudes are given as planetocentric). The SEB is a
11 site of intense convective activity and lightning storms (Ingersoll et al., 2004), and
12 is one of the few locations where spectroscopically identifiable ammonia clouds
13 (SIACs, Baines et al., 2002) have been observed. However, this activity and
14 the dark colouration of the SEB were completely absent when Jupiter emerged
15 from behind the Sun during the 2010 apparition, replaced by the pale 'faded'
16 state (Fig. 2c). This missing jovian belt captured the imagination of amateur and
17 professional astronomers alike, and it prompted a program of thermal infrared
18 imaging of Jupiter's faded SEB from the ESO Very Large Telescope (VLT) at
19 Cerro Paranal in Chile. These data, along with supporting observations from the
20 NASA Infrared Telescope Facility (IRTF) and amateur observers, will be used
21 to determine the variations in temperature and aerosol opacity within the SEB
22 between 2008 and 2010 and provide insights into the underlying physicochemical

23 mechanisms responsible for these dramatic modifications to Jupiter's appearance.

24 The SEB fade and revival cycles appear to follow a repeatable pattern, albeit
25 at irregular and unpredictable intervals because the underlying physical causes
26 are unknown. Excellent historical accounts of the SEB life cycle at visible wave-
27 lengths can be found in Peek (1958), Rogers (1995) and Sanchez-Lavega and
28 Gomez (1996). The 2009-2010 fade is the start of the fifth SEB life cycle since
29 the first spacecraft encounter with Jupiter (Pioneer 10 in December 1973), and
30 the first to be investigated in detail in the thermal infrared using the high spatial
31 resolutions and broad wavelength coverage of modern telescopes and instrumen-
32 tation. Pioneer 10 and 11 visited Jupiter during the 1972-1975 faded state prior to
33 the July 1975 revival (Rogers, 1995; Orton et al., 1981). After a 14-year hiatus,
34 the SEB faded and revived in 1989-1990 (Yanamandra-Fisher et al., 1992; Kuehn
35 and Beebe, 1993; Satoh and Kawabata, 1994) and 1992-1993 (Sanchez-Lavega
36 et al., 1996; Moreno et al., 1997). The next 'partial' fade began in 2007: New
37 Horizons observations in January-February 2007 revealed the absence of both the
38 chaotic turbulence and fresh NH_3 ice clouds northwest of the GRS (Reuter et al.,
39 2007; Baines et al., 2007), but retrievals of cloud opacity from VLT/VISIR still
40 demonstrated a cloud-free SEB (Fletcher et al., 2010b). A fade had started, but
41 a violent revival began much earlier than expected, restoring dark coloration and
42 turbulent activity by the end of 2007 (Rogers, 2007a,b). This study concerns the
43 fading event between May 2009 and July 2010.

44 The general pattern of the SEB life cycle can be summarised as follows. Af-
45 ter the cessation of turbulent rifting and convective events to the northwest of the
46 GRS, the SEB (7-17°S planetocentric latitude) fades to a pale colour over a mat-
47 ter of months, obscuring the southern component of the SEB (SEBs, 15-17°S)

48 and leaving a narrow northern component (SEBn, 7-10°S) which has also been
49 observed to fade in some years. During this unusual phase the GRS appears as a
50 conspicuous red oval surrounded by white aerosols. The faded state can persist for
51 1-3 years before a spectacular revival begins with a single, localised disturbance
52 (the SEBD). Vigorous eruptions generate complex patterns with bright and dark
53 coloration throughout the SEB, encircling the planet and ultimately restoring the
54 typical brown colour.

55 The aim of this research is to reconcile physicochemical variability (temper-
56 atures, composition, clouds) derived from 7-20 μm VLT imaging with visible
57 changes in the albedo of the SEB. The vertical temperature structure and spatial
58 distribution of aerosols during the fade are used to differentiate between different
59 mechanisms for the ‘disappearance’ of the SEB. Section 2 introduces the sources
60 of infrared and visible data and the techniques used to determine temperatures
61 and aerosol opacities. Section 3 presents a timeline for the 2009-2010 fade, which
62 is used to provide insights into the underlying mechanisms for the SEB fade in
63 Section 4.

64 **2. Observations and Analysis**

65 *2.1. VLT Imaging*

66 High spatial resolution imaging of Jupiter in the Q (17-20 μm) and N (8-
67 14 μm) bands from the ESO Very Large Telescope (VLT) mid-infrared cam-
68 era/spectrograph (VISIR, Lagage et al., 2004) was previously used to probe the
69 atmospheric structure of Jupiter’s Great Red Spot (Fletcher et al., 2010b) and to
70 study the aftermath of the 2009 asteroidal collision (Orton et al., 2011; Fletcher
71 et al., 2010a). We were awarded four hours of Directors Discretionary Time

72 (program 285.C-5024A) to characterise the structure and composition of Jupiter's
73 faded SEB in July 2010, which we compare to previous VISIR observations ac-
74 quired between May 2008 and November 2009 (Table 1) using identical imaging
75 techniques.

76 Jupiter is too large to fit entirely within the VISIR field of view ($32'' \times 32''$),
77 so northern and southern hemispheres were imaged separately, often on different
78 dates. Furthermore, thermal imaging requires chopping between the target and
79 an off-source position to detect the jovian flux on top of the background telluric
80 emission. However, the maximum chopping amplitude of VLT/VISIR is limited
81 to $25''$, meaning that some of the 'sky' image is obscured by the planet, preventing
82 the use of some regions of the chopped-differenced image (e.g., white regions re-
83 moved from $8.6\text{-}\mu\text{m}$ images in Fig. 1). Further background stability was achieved
84 by offsetting the telescope to a sky position $60''$ from Jupiter (nodding).

85 An imaging sequence typically featured eight filters (Table 2) sensitive to
86 (a) atmospheric temperatures via the collision-induced hydrogen continuum and
87 stratospheric hydrocarbon emission; and (b) tropospheric ammonia and aerosols
88 (8.59 and $10.77\ \mu\text{m}$). Each filter was observed twice, with a small $1\text{-}2''$ dither to fill
89 in bad pixels on the detector for all eight filters. A full imaging sequence required
90 approximately 40 minutes. The ESO data pipeline was used for initial reduction
91 and bad-pixel removal via its front-end interface, GASGANO (version 2.3.0¹).
92 Images were geometrically registered, cylindrically reprojected and absolutely
93 calibrated using the techniques developed in Fletcher et al. (2009b). Radiomet-
94 ric calibration was achieved by scaling the observations to match Cassini/CIRS

¹<http://www.eso.org/sci/data-processing/software/gasgano/>

95 measurements of Jupiter's radiance acquired during the 2000 flyby (Flasar et al.,
96 2004). Consequently we cannot investigate *absolute* changes in Jupiter's infrared
97 emission, but we can study *relative* variability between different latitudinal bands
98 (see Fletcher et al., 2009b, for a complete discussion). Measurement errors of
99 approximately 4-6% for each filter were estimated from the variability of the sky
100 background in each image. All latitudes in this study are planetocentric, all longi-
101 tudes are quoted for Jupiter's System III West (using the standard IAU definition
102 of System III rotation (1965), recently reviewed by Russell and Dougherty, 2010).

103 Examples of the VISIR imaging at $8.6\ \mu\text{m}$ between May 2008 and July 2010
104 (where low fluxes indicate either elevated aerosol opacities or cool atmospheric
105 temperatures) are shown in Figs. 1 and 2. These are compared to examples of
106 amateur images at visible wavelengths and Jupiter's $4.8\text{-}\mu\text{m}$ emission on dates
107 close to those of the VISIR observations obtained by NASA's Infrared Telescope
108 Facility NSFCAM2 instrument (Table 3). Jupiter's $4.8\text{-}\mu\text{m}$ emission is attenuated
109 by aerosols above the 2-3 bar level, so dark regions indicate locations of higher
110 opacity. Although the dates and spatial coverage of the mid-IR and $4.8\text{-}\mu\text{m}$ images
111 differ, their zonal properties can be compared to provide insights into the vertical
112 distribution of cloud opacity during the fade sequence (Section 3).

113 2.2. *Mid-IR Retrievals*

114 To separate the effects of temperature, aerosol opacity and composition on
115 the VISIR filtered imaging, cylindrical radiance maps in eight filters (7.9 , 8.6 ,
116 10.8 , 12.3 , 13.0 , 17.7 , 18.7 and $19.5\ \mu\text{m}$) were stacked to form rudimentary image
117 cubes using the procedure described by Fletcher et al. (2009b). The tempera-
118 ture structure, composition and aerosol distribution were derived from the 8-point
119 spectra using an optimal estimation retrieval algorithm, NEMESIS (Irwin et al.,

120 2008). Sources of spectral line data; conversion of line data to k -distributions
121 and Jupiter's *a priori* atmospheric structure were described in detail by Fletcher
122 et al. (2011). Two different retrieval approaches were tested: (i) a single-stage
123 process retrieving $T(p)$, NH_3 , C_2H_6 and aerosol opacity simultaneously, and (ii)
124 a two-stage process deriving temperatures first (from the $7.9 \mu\text{m}$ and $13.0\text{-}19.5$
125 μm filters) before the retrieval of composition. Atmospheric temperatures were
126 derived as a vertical profile defined on a grid of 80 layers between 10 bar and
127 0.1 mbar, whereas Cassini-derived profiles of aerosol opacity, NH_3 and C_2H_6
128 (Fletcher et al., 2009a; Nixon et al., 2007) were simply scaled to reproduce the
129 VISIR spectra. The two-stage process was found to produce unreliable results be-
130 cause the competing effects of temperature and aerosol opacity were inseparable
131 without using all 8 filters simultaneously. Thus the single-stage retrieval was used
132 for each of the observations in Table 1.

133 Radiances from each observation in Table 1 were averaged over a 10° -longitude
134 range surrounding the central meridian, and interpolated onto a 1° latitude grid.
135 Care was taken to avoid large ovals (the GRS, Oval BA) to prevent spurious re-
136 sults, such that central meridian scans are representative of the zonal mean radi-
137 ances on each date. Atmospheric temperatures, aerosol opacity and the distribu-
138 tions of tropospheric NH_3 and stratospheric C_2H_6 were retrieved simultaneously
139 for each latitude to determine meridional variations in each quantity. Examples of
140 the quality of the 8-point spectral fits at each latitude are shown in Fig. 3, which
141 compares synthetic radiances with measurements at the centre of the SEB (12.5°S)
142 on three different dates. Calibrated radiances were similar for all three epochs,
143 with evidence of a decrease in emission at 13.0 and $8.6 \mu\text{m}$ between 2008 and
144 2010. Conversely, variations of zonal mean radiances at 10.8 and $12.3 \mu\text{m}$ (sen-

145 sitive to NH_3 and C_2H_6 respectively) were negligible, suggesting that the VISIR
146 photometry does not show evidence for NH_3 or C_2H_6 variability during the fade.
147 It is likely that detection of gaseous variability during an SEB life cycle would
148 require spectroscopy rather than photometry. Nevertheless, atmospheric temper-
149 atures and aerosols could be reliably separated using the 8-point spectra and will
150 be discussed in Section 3.

151 The retrieved haze opacity is driven by the $8.6\text{-}\mu\text{m}$ brightness temperatures
152 plotted on the left of Figs. 1-2, where lower brightness temperatures are the re-
153 sult of higher aerosol opacities. However, the 8-point spectra lack the informa-
154 tion content required to determine the vertical distribution of this aerosol opacity.
155 Cassini/CIRS spectral analyses (Wong et al., 2004; Matcheva et al., 2005; Fletcher
156 et al., 2009a) demonstrated that the $8\text{-}11\ \mu\text{m}$ wavelength range was best repro-
157 duced by a compact cloud layer of $10\text{-}\mu\text{m}$ radius NH_3 ice particles near 800 mbar,
158 although neither the composition nor the altitude of these aerosols were particu-
159 larly well constrained. Using the CIRS-derived aerosol distribution, we scale the
160 cumulative optical depth of the aerosols above the 800-mbar level to reproduce
161 the 8-point spectra at each latitude.

162 **3. Results: The SEB Fade Timeline**

163 This following sections compare temperature and aerosol distributions derived
164 from VLT $7\text{-}20\ \mu\text{m}$ filtered imaging to both IRTF $4.8\text{-}\mu\text{m}$ images of deep cloud
165 opacity and amateur imaging of the visible coloration to reveal the sequence of
166 changes occurring during the SEB fade. The timeline of SEB changes between
167 2008 and 2010 is summarised in Table 4, along with a selection of key character-
168 istics of the fade in Table 5.

169 *3.1. Initial State of the SEB (Pre-May 2009)*

170 Filamentary turbulent convective activity usually dominates the SEB to the
171 northwest of the Great Red Spot (GRS) in a region known as the ‘GRS wake.’ The
172 chaotic activity is driven by the convergence of a system of complex atmospheric
173 flows, where retrograde flow (from the east) at 17°S is deflected northward around
174 the periphery of the GRS to meet the prograde flow (from the west) at 7°S. This
175 typical state was observed throughout 2008 (Fig. 1a-b), where the SEB between
176 7-17°S has a higher temperature than the equatorial zone (EZ) to the north and the
177 South Tropical Zone (STrZ) to the south. Cloud opacity measured at both 4.8 and
178 8.6 μm is typically low, so that the SEB appears relatively bright at both of these
179 wavelengths. This is consistent with the typical view of upper tropospheric belt-
180 zone circulation (e.g., Ingersoll et al., 2004) whereby air rises at the equator and
181 subsides over the neighbouring belts, creating warm, cloud-free and volatile de-
182 pleted conditions within the SEB and NEB (North Equatorial Belt). Small white
183 spots and rifting observed in the visible in Fig. 1a-b coincide with higher aerosol
184 opacities at 8.6 μm and cooler tropospheric temperatures, indicating localised up-
185 welling within the generally subsiding belt. Such upwelling transports spectro-
186 scopically identifiable NH_3 ice (SIACs, Baines et al., 2002) upwards into the GRS
187 wake region.

188 Table 4 shows that this SEB activity continued until May-June 2009, when am-
189 ateur imaging revealed the absence of any convective white spots (Rogers, 2010a),
190 just prior to the first mid-IR images in July 2009 (Fig. 1c). Although the cause
191 of this inhibition of convective activity cannot be identified in the time sequence
192 presented here, it signalled the start of a remarkable transformation in the SEB
193 over the following 12 months.

194 3.2. *Formation of the SEBZ (July-August 2009):*

195 A comparison of the visible, 8.6 and 4.8- μm images in July 2009 (Fig. 1c)
196 shows a substantial alteration to the distribution of aerosol opacity within the SEB
197 at a time when the visible colours of the SEB were largely unaltered. At this
198 time, the SEB had a pale interior separating a narrow brown northern component
199 (the SEBn, 7-10°S) and a broad brown southern component (the SEBs, 14-18°S).
200 Because there is minimal gas opacity at 4.8 μm , strong thermal emission implies
201 a relative dearth of aerosol opacity above the 2-3 bar pressure level (e.g., Roos-
202 Serote et al., 1998); whereas 8.6- μm is sensitive only to clouds and hazes above
203 the 800-mbar level. An enhancement in cloud opacity above the 2-3 bar level in
204 June-July 2009 caused a substantial reduction in 4.8- μm emission from the SEB,
205 restricting cloud-free conditions to the SEBn and SEBs. The transformation at 8.6
206 μm was equally dramatic - the fine structures that characterised the VISIR 8.6- μm
207 imaging in 2008 had been replaced by a more diffuse appearance, with a narrow
208 dark lane (8-13°S) of elevated opacity at the 800-mbar level. This lane of elevated
209 aerosol opacity is known as the SEB zone (SEBZ).

210 Fig. 4 shows how the establishment of the SEBZ modified central-meridian
211 brightness temperatures across the SEB between 2008 and 2010. These bright-
212 ness temperatures are averaged within 10° longitude of the central meridian for
213 each filter, so are not true zonal averages. Hence, some of the apparent variabil-
214 ity results from the presence of discrete features (waves, vortices) close to the
215 central meridian. Changes associated with the SEB fade between 7 and 20°S are
216 most dramatic at 8.6 μm , with the whole region becoming darker in 2009-2010
217 than the south temperate region poleward of 25°S. Variations at other wavelengths
218 are more subtle: filters with contribution functions sensitive to upper tropospheric

219 temperatures (150-300 mbar, approximately, for 17.6 and 18.7 μm , Table 2) re-
220 mained largely unchanged throughout the fade sequence when compared to mid-
221 IR variability at other latitudes. Conversely, close inspection of images probing
222 higher pressures ($p > 300$ mbar: 8.6, 10.8, 13.0 and 19.5 μm) demonstrate the
223 development of a multi-peaked structure, with radiance maxima at 9°S (SEBn)
224 and 15-17°S (SEBs), and a zone-like minimum at 12°S (the SEBZ). The transi-
225 tion from the turbulent SEB to the cool SEBZ by late 2009 is clearly shown in
226 maps of 10.8- μm brightness temperatures (Fig. 5), sensitive to temperatures and
227 ammonia near the 400-mbar level.

228 3.2.1. SEBZ Temperatures

229 The changes in the mid-IR radiance in Fig. 4 manifest themselves as variations
230 in the retrieved tropospheric temperatures in Fig. 6, particularly those at high
231 pressures (480 and 630 mbar in the panels f and h), indicating a difference in the
232 latitudinal temperature gradient between 2008 and 2009-10. Uncertainties in the
233 absolute calibration of the VISIR images, combined with the broad pressure range
234 covered by the weighting function for each filter (Fletcher et al., 2009b) and the
235 degeneracies between temperature and composition, lead to considerable retrieval
236 uncertainties for temperatures at $p > 500$ mbar in Fig. 6e-h, so that *absolute*
237 cooling is difficult to detect at the SEB latitude. On the other hand, the presence
238 of the distinct cool zone (SEBZ) from 2009 onwards, *relative* to the warmer SEBn
239 and SEBs, can be seen at 480 and 630 mbar in Figs. 6f-h. Temperature contrasts
240 of 1.0 ± 0.5 K between the SEBZ and the northern and southern components were
241 measured at 630 mbar in July 2010 (Fig. 6h). Of the three Q-band filters in Fig.
242 4, only the deep-sensing 19.5- μm filter (which has the lowest diffraction-limited
243 resolution of all the images used in this study) detected the SEBZ, confirming

244 that the SEBZ formation occurred at depth. The cool SEBZ was not observed
245 at lower pressures (150-300 mbar) sensed by 17.6- and 18.7- μm filters where the
246 SEB retained its usual warm belt-like conditions.

247 Indeed, the temperature fluctuations in the stable upper troposphere between
248 15-300 mbar were small compared to those at other latitudes, particularly those
249 associated with the NEB (see Appendix A). The SEBZ formation at depth did
250 have a subtle effect at these lower pressures - both the retrieved temperatures near
251 240 mbar (Fig. 6d) and the raw radiances (Fig. 4) demonstrate a ‘flattening’ of the
252 meridional temperature gradient (dT/dy) between 7-20°S as the fade progressed.
253 Instead of having a belt with a peak temperature in the centre (12°S), the 240-
254 mbar temperatures during the faded state became more homogenised with latitude
255 (dT/dy tends to zero between 10-15°S at 240 mbar, Fig. 6d). As vertical shears on
256 the zonal wind (du/dz) are related to dT/dy by the geostrophic thermal windshear
257 equation, this reduction of dT/dy in 2009-10 compared to the normal state of the
258 SEB suggests a reduction in the windshear on both the prograde jet at 7°S and the
259 retrograde jet at 17°S in the troposphere. Zonal flow associated with these two
260 opposing jets could therefore persist to higher altitudes (i.e., near the tropopause)
261 during a faded state than during the ‘normal’ state.

262 Finally, stratospheric temperatures above the SEB show considerable variabil-
263 ity between 2008 and 2010 (Fig. 6a) as part of Jupiter’s Quasi Quadrennial Os-
264 cillation (QOO, Leovy et al., 1991), which affects the stratospheric temperatures
265 between 20°N and 20°S with a period of 4-5 years. However, no causal connec-
266 tion between the fades and the stratospheric oscillation is found: (i) the regularity
267 of the QOO means that it cannot be responsible for the SEB fades when some
268 are separated by 14 years or more; and (ii) the 2009-10 observations show the

269 stratospheric SEB warmer than the EZ, whereas data in 1989-90 and 1992-93
270 (Friedson, 1999) show the reverse to be true. We conclude that the SEB fade had
271 no effect on stratospheric temperatures near 5 mbar.

272 3.2.2. *SEBZ Aerosols*

273 Table 4 indicates that changes to the infrared aerosol opacity at 4.8 and 8.6 μm
274 in July-August 2009, as well as the formation of the cool SEBZ at $p > 300$ mbar,
275 occurred several months before the greatest degree of visible whitening of the SEB
276 was observed in April 2010. Furthermore, opacity variations at 4.8 and 8.6 μm
277 (Figs. 1-2) were morphologically different and proceeded at different rates. Varia-
278 tions in cloud opacity above the 2-3 bar level are shown in the latitudinal variations
279 of 4.8- μm emission (Fig. 7) extracted from NSFCAM2 images (Table 3). Radi-
280 ances were extracted within 10° of the central meridian for each image and have
281 been normalised to the equator ($\pm 5^\circ$) for ease of comparison. Between 2008 and
282 2010 an extreme asymmetry developed between the SEB and NEB (which was
283 also undergoing changes in emission, see Appendix A), with a notable change
284 in contrast between the bright SEBn and the dimmer SEBs occurring between
285 July and August 2009 (Figs. 1-2), coincident with the first VLT observations of
286 the SEBZ. The 4.8- μm radiance of the SEBs at 16-18°S diminished steadily from
287 July-August 2009 onwards. By the time of the first NSFCAM2 observations in
288 June 2010, by which time the SEB visible whitening was complete, the SEBs
289 emission had vanished in its entirety and the SEBn emission was substantially re-
290 duced, a state that persisted until at least September 2010 (the final NSFCAM2
291 observations of this study).

292 Opacity variations at lower pressures ($p < 800$ mbar) sensed by VISIR were
293 separated from thermal variations by the NEMESIS retrievals described in Sec-

tion 2.2. Fig. 8 shows the latitudinal variation of the cumulative opacity above the 800-mbar level, with the SEB region highlighted by a dashed box. Opacities of the SEB and NEB were similar in 2008 (a factor of 2 smaller than the equatorial opacity), but the SEB opacity then increased dramatically between 2009 and 2010. By July 2010, the SEB opacity was 90% of that in the EZ (Equatorial Zone), compared to 50% in 2008. This was caused by an increased opacity of 80% compared to September 2008. The dramatic ‘clouding-over’ of the SEB is most apparent in Fig. 10, where aerosol opacity was retrieved from 8-point spectra on a $0.5 \times 0.5^\circ$ grid. Retrieved aerosol opacities in September 2008 showed the GRS as an isolated vortex of high aerosol opacity (Fig. 10a), with cloud-free conditions over the SEB caused by wide-spread subsidence (similar cloud-free conditions were previously identified by Fletcher et al., 2010b, throughout much of the 2000-2008 period). But by November 2009 the clouds over the SEB had become distinctly more opaque; and by July 2010 the majority of the SEB interior had the same opacity as the STrZ (South Tropical Zone), separated from the adjacent bands by a narrow cloud-free SEBs and wider SEBn (Fig. 10c).

The SEBn ($7-10^\circ$ in Fig. 8) remained cloud-free throughout the fade, with only a small rise in opacity consistent with the detection of SEBn $4.8\text{-}\mu\text{m}$ emission (albeit attenuated) in 2010 (Fig. 7). The SEBs was observed as a diffuse band at $8.6\ \mu\text{m}$ in July-August 2009 (Fig. 2a), but its opacity had increased dramatically by November 2009 (Fig. 2b). This transition at $8.6\ \mu\text{m}$ coincided with the initial visible fading of the SEBs and the disappearance of $4.8\text{-}\mu\text{m}$ emission (Table 4). Finally, although Figs. 2c and 10c suggest that the SEBs opacity had decreased again in July 2010 (it can be seen as a narrow, bright $8.6\text{-}\mu\text{m}$ streak west of the GRS), this was almost certainly a temporary event associated with a narrow,

319 visibly-dark streak emanating from the bright plume north of the GRS (visible in
320 Fig. 2c as a spot of high 8.6- μm opacity).

321 The differences between 4.8- and 8.6- μm aerosol opacity are evident in both
322 July 2009 and July 2010. At the start of the fade in 2009 (Fig. 1c) 4.8- μm opacity
323 was restricted to narrow bands in the SEBn and SEBs, whereas 8.6- μm opacity
324 was much broader. By the completion of the fade in July 2010 (Fig. 2c), 4.8-
325 μm emission from the SEBs was undetectable, whereas it could be faintly distin-
326 guished at 8.6 μm . The attenuation of 4.8- μm flux cannot be solely explained by
327 the increased opacity retrieved from the 8.6- μm filter. These differences suggest
328 sensitivity to two different populations of cloud and aerosol particles: an upper
329 cloud with greater transparency near the SEBn and SEBs, and a deeper cloud with
330 opacity completely obscuring the bulk of the SEB and the SEBs. This implies
331 that the circulation regimes associated with the faded SEB varied with height,
332 with subsidence causing cloud-clearing over the SEBs at $p < 800$ mbar but not
333 at $p > 800$ mbar. Modelling of simultaneous 4.8-20 μm spectroscopy (at low to
334 moderate resolutions) will be required to separate these different vertical regimes.

335 3.3. Lifetime of the Brown Barges (June 2009-July 2010)

336 Between June and August 2009, a series of five dark brown cyclonic ovals
337 ('barges', B1-B5) formed to the west of the GRS (Rogers, 2010a) at 15-16°S
338 (Figs. 1-2). They formed within the broad SEBs, which was still visible as a pale
339 orange band between 14-18°S during this interval and displayed warmer temper-
340 atures than the SEBZ to the north (Fig. 9d). The first barge, B1, appeared on June
341 15, just west of the GRS (visible in Fig. 1c). Four others then appeared at pro-
342 gressively higher longitudes, with B5 the last to appear on August 4. These barges
343 may be manifestations of a deeper underlying circulation, and had not been visible

344 in the preceding convective state of the SEB. They have not been frequently ob-
345 served during previous SEB fades (summarised by Sanchez-Lavega and Gomez,
346 1996), but the 2007 revival (following the partial fade) may have started with a
347 convective plume within one such barge (Rogers, 2007b), suggesting an impor-
348 tant role for these barges in the upcoming revival. The barges were bright at both
349 4.8 and 8.6 μm , and the retrieved aerosol opacity above the 800-mbar level (Fig.
350 10) suggests that they were isolated cloud-free regions of strong atmospheric sub-
351 sidence embedded within the uniformly-opaque SEBs. This atmospheric subsi-
352 dence warms the air within the barges, making them warmer than the surrounding
353 SEBs (Fig. 5, sensitive to temperatures near 400 mbar, and retrieved temperature
354 maps in Fig. 9). The barges were not visible in Q-band imaging sensitive to lower
355 pressures, and do not perturb temperatures in the 240-mbar region (Fig. 9c).

356 When Jupiter reappeared from behind the Sun in 2010 amateur observers re-
357 ported the continued presence of these barges (Rogers, 2010a). By July 2010
358 (Table 4) the barges had also faded, replaced by faint blue-grey spots that marked
359 the northeast corners of their original locations (Rogers et al., 2010). Fig. 5c
360 shows that the underlying warm cyclonic circulation of barge B1 was still present
361 on July 13th, even though only a diffuse remnant of the barge could be detected
362 at 8.6 μm (Fig. 2c). No evidence for the barges was detected at 4.8 μm (i.e., the
363 radiance was completely attenuated due to aerosol opacity), and B1 could not be
364 clearly identified in the aerosol map in Fig. 10c, so we can conclude that although
365 the barges had also faded by July 2010, the original circulation may persist below
366 the visible clouds.

367 *3.4. Completion of the Fade (October 2009-July 2010)*

368 By April 2010 the opacity of the SEB had increased dramatically (Fig. 10)
369 and the belt was very pale in visible light. The SEBn had narrowed between
370 November 2009 and July 2010 but remained present (similar to the faded state of
371 1992, Sanchez-Lavega et al., 1996), and could be identified as a bright band at 4.8
372 μm (Fig. 2c). The SEBs had a bright southern edge at 8.6 μm but was completely
373 attenuated at 4.8 μm , and although the warm cyclonic circulation of the barges
374 remained detectable, they produced no colour contrasts in visible light except for
375 the faint blue-grey spots described above.

376 The faded SEB showed no discrete convective activity at any wavelength, al-
377 though the narrow lanes in the SEBn and SEBs exhibited small-scale zonal wave
378 activity to the west of the GRS with a longitudinal wavelength of 5-6°. The SEBn
379 projections (wavy edges or ‘chevrons’ in Figs. 2c) are typical features of this
380 prograde jet at 6-8°S, whereas the SEBs zonal wave activity at 18-20°S is a new
381 feature of the faded state of the belt. This undulating appearance of the SEBs was
382 also imaged during the completely faded state in 1974 (Pioneer-11 images, Rogers
383 and Young, 1977) and 1993 (Sanchez-Lavega et al., 1996); they were not present
384 during the partial fade of 2007 when the SEBs edge was completely straight, and
385 they were not visible in the early stages of the 2009/10 fade (i.e., before October
386 2009). The SEBs undulations were further south than the usual SEBs boundary
387 (see Table 5). Windspeed measurements for the SEBs structures from amateur
388 imaging (Rogers et al., 2010) indicate that their retrograde velocities were con-
389 sistent with spacecraft-derived zonal velocity measured for 19°S (i.e., slower than
390 the retrograde jet peak at 17°, which is usually thought to bound the SEBs).

391 At the time of writing (October 2010) amateurs and professionals are con-

392 tuning to observe Jupiter for signs of a revival of the turbulence and the typical
393 brown appearance of the SEB. In Section 4 we discuss hypotheses for the onset
394 of the SEB fade and the possible thermal-infrared characteristics of the upcoming
395 revival.

396 4. Discussion

397 Retrievals of atmospheric temperature and aerosol opacity from VLT/VISIR
398 imaging have revealed that the increased SEB reflectivity during a fade is accom-
399 panied by (a) the formation of a cool SEBZ in the centre of the typically warm
400 belt for $p > 300$ mbar, separating the northern and southern components and de-
401 creasing the thermal windshear in this region; and (b) a dramatic increase in the
402 opacity of jovian aerosols in the SEB in two vertical regimes: aerosols in a cloud
403 deck near 800 mbar attenuating 8.6- μm radiance, and clouds above the 2-3 bar
404 level attenuating 4.8- μm radiance. By the completion of the fade in July 2010,
405 enhanced aerosol opacity obscured the bulk of the SEB and the SEBs, whereas
406 the SEBn was still visible and relatively cloud-free (typical of previous SEB life
407 cycles, Sanchez-Lavega and Gomez, 1996). The retrieved temperature distribu-
408 tions and the differences between aerosol distributions mapped by the 4.8- and
409 8.6- μm filters confirm that the SEB fade was caused by changes at depth ($p > 300$
410 mbar), most likely within the convective region of the troposphere rather than the
411 stable, radiatively cooled upper troposphere. This deep change is supported by
412 a qualitative inspection of amateur CH₄-band images (0.89 μm) in 2010, which
413 indicated that the upper tropospheric hazes (100-200 mbar) remained unaffected
414 by the fading process (A. Sánchez-Lavega, *pers. comm.*).

415 Thermal-IR observations between the cessation of SEB convective activity in

416 May 2009 and the onset of the fade are crucial to distinguish between two scenar-
417 ios proposed to explain the formation of the cool, optically-thick SEBZ. Firstly,
418 Sanchez-Lavega and Gomez (1996) suggested that the increased reflectivity of the
419 opaque cloudy layer at visible wavelengths would lead to heating below the cloud
420 (a ‘greenhouse effect’ driven by internal radiation ‘trapped’ by the high opac-
421 ity of the cloudy layer) and cooling above, increasing the atmospheric lapse rate
422 $\Gamma = -dT/dz$. In this scenario, the cool SEBZ would begin to form *after* the de-
423 velopment of the thicker reflective clouds. However, the cool SEBZ (Fig. 4) and
424 the thickening infrared aerosol opacity (Figs. 7 and 10) were observed in 2009
425 *before* the complete whitening of the SEB by April 2010, consistent with thermal
426 changes *causing* the fade rather than being a by-product.

427 In a second scenario, the enhanced opacity of the cool SEBZ can be directly
428 compared to conditions in Jupiter’s zones, where upwelling and atmospheric di-
429 vergence brings condensibles like NH_3 and H_2S upward from deeper levels to
430 form clouds of NH_3 and NH_4SH ice (i.e., the SEB takes on zone-like proper-
431 ties, Satoh and Kawabata, 1994). Enrichments in volatiles and/or decreased tro-
432 pospheric temperatures can both increase the density of an ice cloud and move it
433 to deeper pressures (e.g., Weidenschilling and Lewis, 1973; Atreya et al., 1999).
434 This scenario suggests that zone-like upwelling forms the cool SEBZ *before* the
435 visible brightening, injecting fresh volatiles to form or reinforce the condensation
436 cloud decks over the SEB. The most likely candidate for the white aerosols of the
437 faded state is NH_3 ice, which is expected to form the 800-mbar clouds attenuating
438 8.6- μm radiance (e.g., Weidenschilling and Lewis, 1973). By April 2010 the fresh
439 ice coating had masked the blue-absorbing chromophore responsible for the belt’s
440 typical red-brown coloration, without affecting the properties of the upper-level

441 hazes ($p < 300$ mbar). This is consistent with the analyses of visible reflectiv-
442 ity changes during the 1989-93 SEB fades (Kuehn and Beebe, 1993; Satoh and
443 Kawabata, 1992, 1994; Moreno et al., 1997), which revealed that both the optical
444 thickness and the single scattering albedo of a 400-700 mbar cloud layer increased
445 during the fade. The authors suggested that this reinforcement of the cloud deck
446 was been driven by a fresh supply of NH_3 gas (from upward diffusion or convec-
447 tive overshooting Kuehn and Beebe, 1993), condensing on available nucleation
448 sites in this region.

449 The 2009-10 observations show that the SEB life cycle also affects cloud con-
450 densation at pressures greater than 800 mbar, as condensation of NH_3 ice alone
451 cannot explain the different spatial distributions of aerosol opacity at 4.8 and 8.6
452 μm . Other condensibles such as NH_4SH may be responsible for the increased
453 opacity above the 2-3 bar level sensed at 4.8 μm , but neither of these ices have
454 been identified spectroscopically during the present faded state of the SEB - a key
455 challenge for future observations.

456 Studies of temperature changes associated with previous SEB fades have been
457 inconclusive - Yanamandra-Fisher et al. (1992) reported a general SEB cooling
458 prior to the 1989 fade from IRTF observations at 18 μm , but the published survey
459 of Orton et al. (1994) concluded that the 1989-1993 fades had no contempora-
460 neous temperature changes at 250-mbar that were distinguishable from seasonal
461 variations (their Fig. 4). Given that the 2009-10 event only showed SEBZ for-
462 mation at higher pressures, the non-detection of a SEB cooling at 18 μm is un-
463 surprising. Observations near 20 μm should have been sufficient to resolve a cool
464 SEBZ, and indeed Pioneer 10 measured colder SEB 20- μm temperatures in 1973
465 (during the faded state) than Pioneer 11 in December 1974 (preceding the July

466 1975 revival, Orton et al., 1981). However, given the low spatial and temporal
467 resolution of these early observations we cannot confirm that the formation of an
468 SEBZ always precedes the visible whitening.

469 *4.1. Modified SEB Flow*

470 The first detectable sign of the onset of a fade was the cessation of the turbulent
471 rifting to the northwest of the GRS (which normally occurs where the retrograde
472 flow at 17°S is deflected northwards to meet prograde flow at 7°S). These convec-
473 tive disturbances are completely absent during the faded SEB state, which may
474 imply that heat flow from deeper levels (thought to drive convective instabilities)
475 is no longer as efficient. We might speculate that (i) a shift in the latitude of the
476 GRS or (ii) a modification to the vertical extent of the vortex (and thus the extent
477 of the blockage to the easterly and westerly flows) could modify the interaction of
478 the GRS with the surrounding wind field at depth, preventing the discrete chaotic
479 structures from forming. The SEBZ formation and associated fade could then be
480 viewed as an alternative method for transporting energy out of Jupiter's interior
481 in the absence of discrete convective activity. The ubiquitous subsidence over the
482 SEB that normally keeps this region free of opacity sources (see, e.g., Fletcher
483 et al., 2010b) may then decline, permitting the development of the cool SEBZ,
484 enhanced NH₃ condensation and the ultimate whitening of the belt.

485 The central latitude of the GRS is difficult to measure in amateur visible im-
486 ages due to limb-darkening effects, but limb fitting and latitude determinations
487 between 2008 and 2010 suggested that any shifts must be smaller than 0.5°, the
488 standard deviation of the mean GRS planetocentric latitude (19.5°S) as measured

489 by the JUPOS Team² (*pers. comms.*, see acknowledgements). Nevertheless, any
490 shifts in the deep flows could also serve to reconfigure the retrograde SEBs jet
491 into a meandering current, possibly giving rise to the series of five brown barges
492 as near-stationary eddies on the northern side of the jet (Rogers, 2010a). In light
493 of this hypothetical relationship between the dynamics of the GRS and the SEB
494 life cycle, modelling efforts that correctly reproduce the turbulent ‘wake’ of the
495 GRS with a generalised moist convection scheme (particularly the addition of
496 H₂O-driven convection, which has a considerable effect on the dynamics), as well
497 as including variable blockages to the mean flow, are required to interpret the
498 cessation of convective activity.

499 Finally, we can speculate that the cessation of turbulence reflects a deeper
500 change to jovian heat flow and meteorology on long timescales. The existence
501 of such deep meteorological changes (known as ‘global upheavals,’ Rogers, 1995,
502 2007a) has been suggested to account for the fact that SEB cycles are often associ-
503 ated with equally large-scale changes in the equatorial zone and in the NTB (as in
504 2007, though not in 2010), but no physical interpretation has yet been suggested.

505 4.2. *Expectations for the SEB Revival*

506 Based on historical records, the faded SEB could persist for 1 to 3 years
507 (Rogers, 1995; Sanchez-Lavega and Gomez, 1996), and we might expect a tem-
508 perature rise (Orton et al., 1981; Yanamandra-Fisher et al., 1992) prior to the SEB
509 disturbance that will ultimately restore the SEB to its usual dark brown appear-
510 ance. Such a temperature rise would raise the condensation level to higher alti-
511 tudes, and lead to resublimation of the bright ices from their condensation nuclei.

²The database for Jupiter object positions project, www.jupos.org

512 If those nuclei contain the blue-absorbing chromophore responsible for the brown
513 coloration of the belt (West et al., 1986), then this mechanism would predict a
514 slow, gradual revival. However, visible observations show that previous SEB re-
515 vivals are anything but gradual. Instead, they are complex, violent and eruptive
516 in nature, spreading from a single localised source called the SEB disturbance
517 (SEBD, Rogers, 1995; Sanchez-Lavega and Gomez, 1996). This source is similar
518 to convective outbreaks that occur frequently in the normal state of the SEB, but is
519 more energetic, either because the fade process enhances the energy supply avail-
520 able for a subsequent outbreak, or because it provides conditions that make the
521 outbreak self-amplifying. From mass conservation, convective eruptions would
522 be associated with nearby regions of local subsidence, which would cause tem-
523 peratures to rise and NH_3 ices to sublime, revealing the typical brown coloura-
524 tion of the jovian belt. The revival then proceeds by advection of these convective
525 plumes and subsiding regions (the dark ‘columns’ observed during previous SEB
526 revivals, Rogers, 1995) along the zonal currents within the SEB, breaking up the
527 thickened cloud deck. In this latter scenario, a global temperature rise across the
528 SEB during a revival seems unlikely, and temperature enhancements are more
529 likely to be localised in subsiding regions.

530 Local subsidence, atmospheric heating and ‘drying’ (sublimation of the NH_3
531 ice coating) is likely to be responsible for the brown barges observed in the faded
532 SEBs (June 2009-June 2010). The longitudinal regularity of the subsidence within
533 the 5 barges may be the manifestation of a zonally-propagating wave, displacing
534 the white NH_3 -coated aerosols to deeper, warmer pressures where the coating
535 sublimates, revealing the darker colour. The 2007 SEBD (after the partial fade)
536 may have erupted from a brown spot analogous to the barges observed in 2009-10

537 (Rogers, 2007a), and the same may have occurred in 1993 (Sanchez-Lavega and
538 Gomez, 1996) and some previous revivals (Rogers, 1995). If so, then the residual
539 warm cyclonic circulations observed in the SEBs after the brown barges had faded
540 may have an important role to play in the upcoming revival.

541 In summary, the VISIR observations of the 2009-10 fade are consistent with
542 enhanced opacity and a colder SEBZ resulting from upwelling of NH_3 -laden air.
543 Enhanced condensation obscures the blue-absorbing chromophore and whitens
544 the SEB. We predict that the next SEB disturbance and revival will not be preceded
545 by a ubiquitous warming of the whole belt, but that convective outbreaks will have
546 associated regions of warm, dry subsidence, re-sublimating the NH_3 ice and once
547 again revealing Jupiter's typical brown SEB.

548 **5. Conclusions**

549 Mid-infrared imaging from VLT/VISIR has been used to retrieve variations of
550 Jupiter's atmospheric temperature and aerosol opacity during a fade of the South
551 Equatorial Belt (SEB), the most complete whitening of this region since 1992.
552 By comparing the mid-IR observations with IRTF images at $4.8 \mu\text{m}$ and amateur
553 visible images, we can draw the following conclusions:

- 554 1. A dramatic increase in the infrared optical thickness of SEB aerosols oc-
555 curred in June-August 2009 across a range of cloud levels in the 0.8 to 3-
556 bar range (attenuating thermal emission at 4.8 and $8.6 \mu\text{m}$). This preceded
557 the increased visible reflectivity of the SEB by several months. The visible
558 fade of the SEBs started west of the GRS, and had reached the region east
559 of the GRS by October-November 2009. By the completion of the fade in
560 April-July 2010, the tropospheric opacity of SEB aerosols near 800 mbar

561 had increased by 80% compared to their 2008 value, obscuring both the
562 SEBs and the five brown barges that had been present since June 2009. The
563 faded SEB appeared to be remarkably quiescent (i.e., no convective plumes
564 or spots), and only the narrow SEBn remained relatively cloud-free.

565 2. A low-temperature zone formed in the centre of the SEB at $p > 300$ mbar in
566 July-August 2009, after the cessation of turbulent convective activity north-
567 west of the GRS in May 2009, but before the increases in visible albedo.
568 The SEBZ formation was only observed in the convectively-unstable region
569 of the troposphere, but it produced a reduction in the meridional tempera-
570 ture gradient (and hence the thermal windshear on zonal jets) in the 100-300
571 mbar region. The SEB fade had no effect on stratospheric temperatures near
572 5 mbar.

573 3. Condensation of NH_3 ice, supplied by SEBZ upwelling of air laden with
574 condensible volatiles from the deep troposphere, is the leading candidate for
575 the increased opacity of the 800-mbar clouds (obscuring $8.6\text{-}\mu\text{m}$ emission).
576 The enhanced condensation then obscured the blue-absorbing chromophore
577 and whitened the SEB. However, different spatial morphologies of aerosol
578 opacity at 4.8 and $8.6\ \mu\text{m}$ suggest the enhanced opacity of a second, deeper
579 cloud deck (above the 2-3 bar level), possibly consisting of NH_4SH ice, al-
580 though neither ice has been identified spectroscopically. The enhanced con-
581 densation hypothesis is consistent with studies of visible reflectivity during
582 previous SEB life cycles.

583 4. The cessation of turbulent convective activity northwest of the GRS pre-
584 ceded the formation of the SEBZ, brown barges and enhanced aerosol opac-
585 ity. The quiescent state of the 'GRS wake' before the onset of the fade

586 suggests a dynamical connection between the atmospheric flows around the
587 GRS and the SEB life cycle.

588 5. Five brown barges formed in the SEBs in June-August 2009 as it began
589 to fade to a pale orange. These warm cloud-free regions of atmospheric
590 subsidence were almost undetectable by July 2010, but their locations were
591 still marked by warm tropospheric temperatures and faint blue patches in
592 visible light. Historical records suggest that these cyclonic circulations may
593 play an important role in the next SEB revival.

594 The revival of the dark coloration of Jupiter's SEB must involve sublimation
595 of the ices from their condensation nuclei, driven by subsidence and warming of
596 dry (volatile-depleted) air. This dry subsidence is likely to warm the atmosphere
597 in localised regions (dark 'columns') adjacent to convective plumes (bright spots)
598 erupting during the SEB disturbance, presumably driven by instabilities and moist
599 convection at depth. At the time of writing (October 2010), amateurs and profes-
600 sionals alike are monitoring the planet, eagerly awaiting the initial disturbance
601 that will ultimately restore Jupiter's SEB.

602 Future observations of an SEB fade and revival sequence should focus on low
603 to moderate resolution mid-infrared spectroscopy (5-25 μm), spatially resolving
604 the SEB to solve the ambiguity between temperatures, gaseous NH_3 and aerosols
605 inherent in a mid-IR filtered imaging retrieval. Regular monitoring of the life
606 cycles of Jupiter's axisymmetric bands should be a priority for future exploration
607 of Jupiter, given that their different fade and revival cycles have the potential to
608 reveal new information about the formation of belts and zones within Jupiter's
609 dynamic troposphere.

610 **Acknowledgments**

611 Fletcher was supported during this research by a Glasstone Science Fellow-
612 ship at the University of Oxford. We wish to thank the director and staff of the
613 ESO Very Large Telescope for their assistance with the execution of these ob-
614 servations. This investigation was based on observations acquired at the Paranal
615 UT3/Melipal Observatory under Jupiter observing programmes executed between
616 May 2008 and July 2010 (ID in Table 1). We are extremely grateful to all the
617 amateur observers who have contributed to the ongoing coverage of Jupiter, es-
618 pecially those whose images are shown in the Figures: M. Salway, A. Wesley,
619 C. Go, J.P. Prost, T. Barry and R. Chavez. We acknowledge the JUPOS team
620 (Hans-Joerg Mettig, Michel Jacquesson, Gianluigi Adamoli, Marco Vedovato),
621 whose measurements of these images enabled the comparative mapping of these
622 features. VLT and IRTF data were reduced with the assistance of a number of JPL
623 student interns, including E. Otto, N. Reshetnikov, A. Allahverdi, J. Greco, Z.
624 Greene, D. Holt, S. Lai and G. Villar. Furthermore, we thank M. Lystrup for her
625 generous donation of time on the IRTF during the July-August observations. Or-
626 ton and Yanamandra-Fisher carried out part of this research at the Jet Propulsion
627 Laboratory, California Institute of Technology, under a contract with NASA. We
628 are grateful to the staff and telescope operators at the NASA Infrared Telescope
629 Facility operated by the University of Hawaii under Cooperative Agreement No.
630 NCC 5-538 with the NASA Science Mission Directorate of Planetary Astronomy
631 Program. We are grateful to two anonymous reviewers for their constructive com-
632 ments about this manuscript.

633 **Figure Captions**

634 **Figure 1:** The SEB fade sequence May 2008-July 2009, observed by VLT/VISIR
635 at $8.6 \mu\text{m}$ (left, sensitive to aerosol opacity at $p < 800$ mbar); visible light from
636 amateur observers (centre); and IRTF/NSFCAM2 observations at $4.8 \mu\text{m}$ (right,
637 sensitive to aerosols above the 2-3 bar level). Visible images taken as close as pos-
638 sible to the VISIR observations have been provided by M. Salway and A. Wesley.
639 Suppressed emission at both 4.8 and $8.6 \mu\text{m}$ is caused by excess aerosol opacity.
640 NSFCAM2 images were taken on different nights to the VISIR images, and do
641 not show the same longitude range. Turbulent activity is evident in rows (a) and
642 (b) (the ‘wake’ of the GRS), and the chain of three barges (B1-B3) are labelled
643 in the SEBs in row (c). The 2008 conjunction of Oval BA and the GRS can be
644 seen in rows (a) and (b). Large white arcs seen equatorward of 5°S in the $8.6\text{-}\mu\text{m}$
645 images are due to the removal of negative-beam artefacts caused by the small $20''$
646 chopping amplitude.

647 **Figure 2:** The SEB fade sequence August 2009-July 2010, observed by VLT/VISIR
648 at $8.6 \mu\text{m}$ (left, sensitive to aerosol opacity at $p < 800$ mbar); visible light from
649 amateur observers (centre); and IRTF/NSFCAM2 observations at $4.8 \mu\text{m}$ (right,
650 sensitive to aerosols above the 2-3 bar level). Visible images taken as close as
651 possible to the VISIR observations have been provided by T. Barry, C. Go and J.P.
652 Prost. Suppressed emission at both 4.8 and $8.6 \mu\text{m}$ is caused by excess aerosol
653 opacity. NSFCAM2 images were taken on different nights to the VISIR images,
654 and do not show the same longitude range. The chain of three barges (B1-B3) are
655 labelled in the SEBs in row (b). The 2010 conjunction of Oval BA and the GRS
656 can be seen in row (c). Large white arcs seen equatorward of 5°S in the $8.6\text{-}\mu\text{m}$
657 images of row a are due to the removal of negative-beam artefacts caused by the

658 small 20" chopping amplitude, which was increased to 25" in November 2009.

659 **Figure 3:** Comparison of synthetic 8-point spectra (lines) to measured zonal
660 mean radiances (points) at the centre of the SEB (14.5°S) at three different epochs
661 - September 2008 (normal state of the SEB); November 2009 (midway through
662 the fade) and July 2010 (once the fade had completed). The NEMESIS retrieval
663 model is capable of reproducing the measured radiances in all 8 filters. There
664 were few differences in the calibrated radiances between the three epochs, except
665 a cooling trend at 8.6 and 13.1 μm as the fade progressed and 7.9- μm variability
666 due to Jupiter's quasi-quadrennial oscillation (QQO). Radiances in the top panel
667 were converted to brightness temperatures in the bottom panel. The sensitivity of
668 each of the eight filters is described in Table 2.

669 **Figure 4:** Central meridian brightness temperature scans from 2008 to 2010
670 in six of the eight filters observed by VISIR. Northern and southern hemisphere
671 images were not acquired simultaneously, so a gap is present at the equator for the
672 earliest dates (Table 1). The location of the SEB is denoted by vertical dotted lines.
673 The brightness temperatures have been offset from the 2010 measurements (black
674 curve) by arbitrary amounts for clarity. The most dramatic change occurred at 8.6
675 μm (decreased emission due to the increased aerosol opacity over the SEB). The
676 formation of the cool SEBZ is also apparent in filters sensitive to temperatures
677 at $p > 300$ mbar (10.8, 13.0 and 19.5 μm), but only a subtle 'flattening' of the
678 meridional temperatures can be observed at 17.6 and 18.7 μm (sensitive to 150-
679 300 mbar). Brightness temperatures have not been corrected for emission angle,
680 so the general decrease from equator to pole in each filter is the effect of limb
681 darkening.

682 **Figure 5:** Examples of Jupiter's 10.8- μm emission (sensitive to tropospheric

683 temperatures near 600 mbar and ammonia gas abundance) from the southern
684 hemisphere during the 2008-2010 fade. The SEBs appears brighter than the north-
685 ern component in 2009 and 2010, and the dark SEBZ becomes more prominent as
686 the fade progresses (panels b and c). Large white arcs seen equatorward of 5°S in
687 panel (a) and (b) are due to the removal of negative-beam artefacts caused by the
688 small 20" chopping amplitude. The location of the warm brown barges and Oval
689 BA are indicated.

690 **Figure 6:** *Left:* Comparing retrieved meridional temperatures at five different
691 pressure levels for 2008 (dashed line), 2009 (dotted line) and 2010 (solid line).
692 The location of the SEB is denoted by vertical dashed lines. The grey bars repre-
693 sent the formal uncertainty on the retrieved quantities at each altitude (i.e., taking
694 correlations between parameters into account), which appear large because of the
695 limited retrieval capabilities from 8-point spectral retrievals and the uncertainties
696 in absolute calibration. However, relative variability in the quantities are robust
697 (similar variations are seen in each filter), even if the absolute values are uncertain.
698 Some disconnect between northern and southern hemisphere results is apparent at
699 the equator because these observations were acquired on different dates, as shown
700 by the key (top right). *Right:* Close-up views of thermal changes associated with
701 the SEB at 240, 480 and 630 mbar, with offsets of 2 K from the 2008 temperature
702 profiles to highlight differences.

703 **Figure 7:** Central meridian radiance scans at 4.8 μm from IRTF/NSFCAM2
704 (Table 3) from May 2008 to September 2010. All radiances have been normalised
705 to the equator ($\pm 5^\circ$), and then the maximum has been normalised to 1.0. A large
706 asymmetry between the NEB and SEB develops between 2008 and 2010.

707 **Figure 8:** Comparison of spatial distributions of aerosol opacity for 2008

708 (dashed line), 2009 (dotted line) and 2010 (solid line). Opacities retrieved from
709 8-point 7-20 μm imaging are sensitive to aerosols above the 800-mbar level, ten-
710 tatively identified as an NH_3 ice cloud (e.g., Wong et al., 2004; Matcheva et al.,
711 2005). The grey bars represent the formal uncertainty on the retrieved quantities at
712 each altitude. Some disconnect between northern and southern hemisphere results
713 is apparent at the equator because these observations were acquired on different
714 dates. The SEB is highlighted by the dashed-line box which highlights the devel-
715 opment of an asymmetry between the NEB and SEB between 2008 and 2010.

716 **Figure 9:** Retrieved temperature maps at 240 mbar (left) and 480 mbar (right).
717 White ellipses mark regions contaminated by artefacts due to (i) the small chop-
718 ping amplitude used by VLT and (ii) cylindrical reprojections of the images. The
719 cool SEBZ is present in 2009 and 2010 in the 480-mbar maps, but cannot be seen
720 at 240 mbar. The vertical variation of zonal mean temperatures is shown in Fig.
721 6.

722 **Figure 10:** Retrieved maps of aerosol opacity for clouds above the 800-mbar
723 pressure level as the SEB faded. The retrieved optical depth was modelled as the
724 cumulative infrared opacity of 10- μm radius NH_3 -ice particles with a base at 800
725 mbar, although NH_3 has not been spectroscopically identified (see Section 2.2).
726 The increase in aerosol opacity over the SEB is dramatic, with the SEB having the
727 same opacity as the Equatorial Zone (EZ) and the South Tropical Zone (STrZ) by
728 July 2010. Aerosols within the GRS remain separated from these white aerosols
729 by a cloud-free ring. White ellipses mark regions contaminated by artefacts due
730 to (i) the small chopping amplitude used by VLT and (ii) cylindrical reprojections
731 of the images.

732 **Figure 11:** Phenomena in the northern hemisphere between May 2008 and

733 June 2010, observed by VLT/VISIR at $8.6 \mu\text{m}$ (left, sensitive to aerosol opacity at
734 $p < 800 \text{ mbar}$); visible light from amateur observers (centre); and IRTF/NSFCAM2
735 observations at $4.8 \mu\text{m}$ (right, sensitive to aerosols above the 2-3 bar level). Visible
736 images taken as close as possible to the VISIR observations have been provided
737 by A. Wesley, T. Barry, C. Go and R. Chavez. Suppressed emission at both 4.8
738 and $8.6 \mu\text{m}$ is caused by excess aerosol opacity. NSFCAM2 images were taken on
739 different nights to the VISIR images, and do not show the same longitude range.
740 The three epochs show the northward expansion of the NEB and the cloudy con-
741 ditions of the northern Little Red Spot (NN-LRS-1) in 2008 (see Appendix A).
742 Large white arcs in the $8.6\text{-}\mu\text{m}$ images are due to the removal of negative-beam
743 artefacts caused by the small $20''$ chopping amplitude and the reprojection of the
744 edges of the VISIR array.

745 **References**

- 746 Atreya, S. K., Wong, M. H., Owen, T. C., Mahaffy, P. R., Niemann, H. B., de
747 Pater, I., Drossart, P., Encrenaz, T., 1999. A comparison of the atmospheres
748 of Jupiter and Saturn: deep atmospheric composition, cloud structure, vertical
749 mixing, and origin. *Plan. & Space Sci.* 47, 1243–1262.
- 750 Baines, K., Carlson, R., Kamp, L., 2002. Fresh Ammonia Ice Clouds in Jupiter I.
751 Spectroscopic Identification, Spatial Distribution, and Dynamical Implications.
752 *Icarus* 159 (1), 74–94.
- 753 Baines, K. H., Simon-Miller, A. A., Orton, G. S., Weaver, H. A., Lunsford, A.,
754 Momary, T. W., Spencer, J., Cheng, A. F., Reuter, D. C., Jennings, D. E., Glad-
755 stone, G. R., Moore, J., Stern, S. A., Young, L. A., Throop, H., Yanamandra-

- 756 Fisher, P., Fisher, B. M., Hora, J., Ressler, M. E., Oct. 2007. Polar Lightning
757 and Decadal-Scale Cloud Variability on Jupiter. *Science* 318, 226–228.
- 758 Cheng, A. F., Simon-Miller, A. A., Weaver, H. A., Baines, K. H., Orton, G. S.,
759 Yanamandra-Fisher, P. A., Mousis, O., Pantin, E., Vanzi, L., Fletcher, L. N.,
760 Spencer, J. R., Stern, S. A., Clarke, J. T., Mutchler, M. J., Noll, K. S., Jun. 2008.
761 Changing Characteristics of Jupiter’s Little Red SPOT. *Astronomical Journal*
762 135, 2446–2452.
- 763 Flasar, F. M., Kunde, V. G., Achterberg, R. K., Conrath, B. J., Simon-Miller,
764 A. A., Nixon, C. A., Gierasch, P. J., Romani, P. N., Bézard, B., Irwin, P., Bjo-
765 raker, G. L., Brasunas, J. C., Jennings, D. E., Pearl, J. C., Smith, M. D., Orton,
766 G. S., Spilker, L. J., Carlson, R., Calcutt, S. B., Read, P. L., Taylor, F. W.,
767 Parrish, P., Barucci, A., Courtin, R., Coustenis, A., Gautier, D., Lellouch, E.,
768 Marten, A., Prangé, R., Biraud, Y., Fouchet, T., Ferrari, C., Owen, T. C., Ab-
769 bas, M. M., Samuelson, R. E., Raulin, F., Ade, P., Césarsky, C. J., Grossman,
770 K. U., Coradini, A., Jan. 2004. An intense stratospheric jet on Jupiter. *Nature*
771 427, 132–135.
- 772 Fletcher, L. N., Orton, G. S., de Pater, I., Edwards, M., Yanamandra-Fisher, P.,
773 Hammel, H. B., Lisse, C. M., 2011. The Aftermath of the July 2009 Impact
774 on Jupiter: Ammonia, Temperatures and Particulates from Gemini Thermal
775 Infrared Spectroscopy. *Icarus* 211, 568–586.
- 776 Fletcher, L. N., Orton, G. S., de Pater, I., Mousis, O., Dec. 2010a. Jupiter’s
777 stratospheric hydrocarbons and temperatures after the July 2009 impact from
778 VLT infrared spectroscopy. *Astron. Astrophys.* 524, A46+.

- 779 Fletcher, L. N., Orton, G. S., Mousis, O., Yanamandra-Fisher, P., Parrish, P. D.,
780 Irwin, P. G. J., Fisher, B. M., Vanzi, L., Fujiyoshi, T., Fuse, T., Simon-Miller,
781 A. A., Edkins, E., Hayward, T. L., De Buizer, J., Jul. 2010b. Thermal struc-
782 ture and composition of Jupiter's Great Red Spot from high-resolution thermal
783 imaging. *Icarus* 208, 306–328.
- 784 Fletcher, L. N., Orton, G. S., Teanby, N. A., Irwin, P. G. J., Aug. 2009a. Phosphine
785 on Jupiter and Saturn from Cassini/CIRS. *Icarus* 202, 543–564.
- 786 Fletcher, L. N., Orton, G. S., Yanamandra-Fisher, P., Fisher, B. M., Parrish, P. D.,
787 Irwin, P. G. J., Mar. 2009b. Retrievals of atmospheric variables on the gas giants
788 from ground-based mid-infrared imaging. *Icarus* 200, 154–175.
- 789 Friedson, A. J., Jan. 1999. New Observations and Modelling of a QBO-Like Os-
790 cillation in Jupiter's Stratosphere. *Icarus* 137, 34–55.
- 791 Ingersoll, A. P., Dowling, T. E., Gierasch, P. J., Orton, G. S., Read, P. L., Sanchez-
792 Lavega, A., Showman, A. P., Simon-Miller, A. A., Vasavada, A. R., 2004.
793 Dynamics of Jupiter's atmosphere. *Jupiter. The Planet, Satellites and Magne-*
794 *tosphere*, pp. 105–128.
- 795 Irwin, P., Teanby, N., de Kok, R., Fletcher, L., Howett, C., Tsang, C., Wilson, C.,
796 Calcutt, S., Nixon, C., Parrish, P., 2008. The NEMESIS planetary atmosphere
797 radiative transfer and retrieval tool. *Journal of Quantitative Spectroscopy and*
798 *Radiative Transfer* 109 (6), 1136–1150.
- 799 Kuehn, D. M., Beebe, R. F., Feb. 1993. A study of the time variability of Jupiter's
800 atmospheric structure. *Icarus* 101, 282–292.

- 801 Lagage, P. O., Pel, J. W., Authier, M., Belorgey, J., Claret, A., Doucet, C.,
802 Dubreuil, D., Durand, G., Elswijk, E., Girardot, P., Käufel, H. U., Kroes, G.,
803 Lortholary, M., Lussignol, Y., Marchesi, M., Pantin, E., Peletier, R., Pirard,
804 J., Pragt, J., Rio, Y., Schoenmaker, T., Siebenmorgen, R., Silber, A., Smette,
805 A., Sterzik, M., Veyssiere, C., Sep. 2004. Successful Commissioning of VISIR:
806 The Mid-Infrared VLT Instrument. *The Messenger* 117, 12–16.
- 807 Leovy, C. B., Friedson, A. J., Orton, G. S., Dec. 1991. The quasiquadrennial
808 oscillation of Jupiter’s equatorial stratosphere. *Nature* 354, 380–382.
- 809 Matcheva, K., Conrath, B., Gierasch, P., Flasar, F., 2005. The cloud structure of
810 the jovian atmosphere as seen by the Cassini/CIRS experiment. *Icarus* 179 (2),
811 432–448.
- 812 Moreno, F., Molina, A., Ortiz, J. L., Nov. 1997. The 1993 south equatorial belt re-
813 vival and other features in the Jovian atmosphere: an observational perspective.
814 *Astron. Astrophys.* 327, 1253–1261.
- 815 Nixon, C. A., Achterberg, R. K., Conrath, B. J., Irwin, P. G. J., Teanby, N. A.,
816 Fouchet, T., Parrish, P. D., Romani, P. N., Abbas, M., Leclair, A., Strobel, D.,
817 Simon-Miller, A. A., Jennings, D. J., Flasar, F. M., Kunde, V. G., May 2007.
818 Meridional variations of C_2H_2 and C_2H_6 in Jupiter’s atmosphere from Cassini
819 CIRS infrared spectra. *Icarus* 188, 47–71.
- 820 Orton, G. S., Fletcher, L. N., Lisse, C. M., Chodas, P. W., Cheng, A., Yanamandra-
821 Fisher, P. A., Baines, K. H., Fisher, B. M., Wesley, A., Perez-Hoyos, S., de Pa-
822 ter, I., Hammel, H. B., Edwards, M. L., Mousis, O., Marchis, F., Golisch, W.,
823 Sanchez-Lavega, A., Simon-Millerl, A. A., Hueso, R., Momary, T. W., Greene,

- 824 Z., Reshetnikov, N., Otto, E., Villar, G., Lai, S., Wong, M., 2011. The At-
825 mospheric Influence, Size and Asteroidal Nature of the July 2009 Jupiter Im-
826 pactor. *Icarus* 211, 587–602.
- 827 Orton, G. S., Friedson, A. J., Yanamandra-Fisher, P. A., Caldwell, J., Hammel,
828 H. B., Baines, K. H., Bergstralh, J. T., Martin, T. Z., West, R. A., Veeder, Jr.,
829 G. J., Lynch, D. K., Russell, R., Malcom, M. E., Golisch, W. F., Griep, D. M.,
830 Kaminski, C. D., Tokunaga, A. T., Herbst, T., Shure, M., Jul. 1994. Spatial
831 Organization and Time Dependence of Jupiter's Tropospheric Temperatures,
832 1980-1993. *Science* 265, 625–631.
- 833 Orton, G. S., Ingersoll, A. P., Terrile, R. J., Walton, S. R., Aug. 1981. Images of
834 Jupiter from the Pioneer 10 and Pioneer 11 Infrared Radiometers - A compari-
835 son with visible and 5-micron images. *Icarus* 47, 145–158.
- 836 Peek, B. M., 1958. *The Planet Jupiter*. Faber and Faber, London.
- 837 Reuter, D. C., Simon-Miller, A. A., Lunsford, A., Baines, K. H., Cheng, A. F.,
838 Jennings, D. E., Olkin, C. B., Spencer, J. R., Stern, S. A., Weaver, H. A., Young,
839 L. A., Oct. 2007. Jupiter Cloud Composition, Stratification, Convection, and
840 Wave Motion: A View from New Horizons. *Science* 318, 223–225.
- 841 Rogers, J., 1995. *The Giant Planet Jupiter*. Cambridge University Press.
- 842 Rogers, J. H., Jun. 2007a. Jupiter embarks on a 'global upheaval'. *Journal of the*
843 *British Astronomical Association* 117, 113–115.
- 844 Rogers, J. H., Oct. 2007b. The climax of Jupiter's global upheaval. *Journal of the*
845 *British Astronomical Association* 117, 226–230.

- 846 Rogers, J. H., July 2010a. Jupiter in 2009: Interim Report, with new insights into
847 the NTZ disturbance, NEB expansion, and SEB fading.
848 URL <http://www.britastro.org/jupiter/2009report07.htm>
- 849 Rogers, J. H., June 2010b. Jupiter in 2010: BAA Jupiter Section Bulletin.
850 URL <http://www.britastro.org/jupiter/2010report04.htm>
- 851 Rogers, J. H., Adamoli, G., Mettig, H., 2011. Jupiter's high-latitude storms: A
852 little red spot tracked through a jovian year. *Journal of the British Astronomical*
853 *Association* 121 (1).
- 854 Rogers, J. H., Mettig, H., Adamoli, G., Jacquesson, M., Vedovato, M., October
855 2010. Jupiter in 2010: Interim report: Southern hemisphere .
856 URL <http://www.britastro.org/jupiter/2010report08.htm>
- 857 Rogers, J. H., Young, P. J., Apr. 1977. Earth-based and Pioneer observations of
858 Jupiter. *Journal of the British Astronomical Association* 87, 240–251.
- 859 Rogers, O. H., Akutsu, T., Orton, G. S., Dec. 2004. Jupiter in 2000/2001. Part
860 II: Infrared and ultraviolet wavelengths. *Journal of the British Astronomical*
861 *Association* 114, 313.
- 862 Roos-Serote, M., Drossart, P., Encrenaz, T., Lellouch, E., Carlson, R. W., Baines,
863 K. H., Kamp, L., Mehlman, R., Orton, G. S., Calcutt, S., Irwin, P., Taylor, F.,
864 Weir, A., Sep. 1998. Analysis of Jupiter North Equatorial Belt hot spots in the
865 4-5- μ m range from Galileo/near-infrared mapping spectrometer observations:
866 Measurements of cloud opacity, water, and ammonia. *Journal of Geophysical*
867 *Research* 103, 23023–23042.

- 868 Russell, C. T., Dougherty, M. K., May 2010. Magnetic Fields of the Outer Planets.
869 Space Science Reviews 152, 251–269.
- 870 Sanchez-Lavega, A., Gomez, J. M., May 1996. The South Equatorial Belt of
871 Jupiter, I: Its Life Cycle. Icarus 121, 1–17.
- 872 Sanchez-Lavega, A., Gomez, J. M., Lecacheux, J., Colas, F., Miyazaki, I., Parker,
873 D., Guarro, J., May 1996. The South Equatorial Belt of Jupiter, II: The Onset
874 and Development of the 1993 Disturbance. Icarus 121, 18–29.
- 875 Sánchez-Lavega, A., Orton, G. S., Hueso, R., García-Melendo, E., Pérez-Hoyos,
876 S., Simon-Miller, A., Rojas, J. F., Gómez, J. M., Yanamandra-Fisher, P.,
877 Fletcher, L., Joels, J., Kemerer, J., Hora, J., Karkoschka, E., de Pater, I., Wong,
878 M. H., Marcus, P. S., Pinilla-Alonso, N., Carvalho, F., Go, C., Parker, D., Sal-
879 way, M., Valimberti, M., Wesley, A., Pujic, Z., Jan. 2008. Depth of a strong
880 jovian jet from a planetary-scale disturbance driven by storms. Nature 451,
881 437–440.
- 882 Satoh, T., Kawabata, K., Jan. 1992. Methane band photometry of the faded South
883 Equatorial Belt of Jupiter. ApJ 384, 298–304.
- 884 Satoh, T., Kawabata, K., Apr. 1994. A change of upper cloud structure in Jupiter's
885 South Equatorial Belt during the 1989-1990 event. Journal of Geophysical Re-
886 search 99, 8425–8440.
- 887 Weidenschilling, S. J., Lewis, J. S., 1973. Atmospheric and cloud structures of the
888 jovian planets. Icarus 20, 465–476.

- 889 West, R. A., Strobel, D. F., Tomasko, M. G., 1986. Clouds, aerosols, and photo-
890 chemistry in the Jovian atmosphere. *Icarus* 65, 161–217.
- 891 Wong, M. H., Bjoraker, G. L., Smith, M. D., Flasar, F. M., Nixon, C. A., 2004.
892 Identification of the 10- μ m ammonia ice feature on Jupiter. *Plan. & Space Sci.*
893 52, 385–395.
- 894 Yanamandra-Fisher, P., Orton, G., Friedson, J., Jun. 1992. Time Dependence of
895 Jupiter's Tropospheric Temperatures and Cloud Properties: The 1989 SEB Dis-
896 turbance. In: *Bulletin of the American Astronomical Society*. Vol. 24 of *Bulletin*
897 *of the American Astronomical Society*. p. 1039.

Table 1: VLT/VISIR Observations of Jupiter's Belts. UT times are approximate, as each filter sequence required approximately 45 minutes to execute.

Date	Hemisphere	Time (UT)	Programme ID
2010-07-13	S	08:10	285.C-5024(A)
2010-06-23	N	08:50	285.C-5024(A)
2009-11-12	S	01:30	084.C-0206(B)
2009-08-10	N	03:00	383.C-0161(A)
2009-08-11	S	02:30	383.C-0161(A)
2009-08-12	S	03:00	383.C-0161(A)
2009-07-24	S	03:30	283.C-5043(A)
2008-09-03	S	04:00	081.C-0137(C)
2008-09-01	N	02:00	081.C-0137(B)
2008-05-17	S	10:00	381.C-0134(A)

Table 2: VLT/VISIR Filters used in this study. Approximate peaks of the filter contribution functions are based on Fletcher et al. (2009b).

Name	Wavelength (μm)	Sensitivity	Approx. Pressure (mbar)
J7.9	7.90	Stratospheric $T(p)$	5
PAH1	8.59	Aerosols and $T(p)$	650
SIV2	10.77	NH_3 , aerosols, $T(p)$	400
NeII_1	12.27	Stratospheric $T(p)$ and C_2H_6	6
NeII_2	13.04	Tropospheric $T(p)$	460
Q1	17.65	Tropospheric $T(p)$	200
Q2	18.72	Tropospheric $T(p)$	270
Q3	19.50	Tropospheric $T(p)$	400

Table 3: NSFCAM2 4.8- μm data used in this study

Date	Time (UT)	Central Meridian
2008-05-27	13:53:39	334.9
2008-06-16	13:45:26	103.3
2008-07-10	13:06:44	96.1
2008-07-27	12:52:05	224.6
2008-08-07	07:22:50	145.9
2008-09-24	06:22:15	133.2
2009-07-20	14:09:23	27.6
2009-08-06	10:30:41	296.9
2009-08-18	13:19:15	46.9
2009-08-27	13:45:42	338.8
2010-06-24	15:50:41	319.9
2010-06-30	14:15:45	85.9
2010-07-01	15:47:43	292.1
2010-09-03	08:26:22	305.4
2010-09-05	10:04:33	306.1

Table 4: Timeline of events in the 2009-2010 Fade

Date	Event	Possible Implication
2008-Sep	Typical state of SEB (Fig. 1a): visibly brown, warm troposphere and cloud-free; turbulent activity NW of the GRS	Subsidence over much of the SEB, localised convective upwelling.
2009-May-26	Turbulent convection NW of the GRS had largely ceased (Fig. 1c)	Inhibition of discrete convective upwelling by some mechanism.
2009-Jun-05	Final bright convective spots observed NW of the GRS, SEB still appears visibly brown	Cessation of SEB turbulence complete.
2009-Jun-15	First dark brown cyclonic barge (B1) appeared west of the GRS (Rogers, 2010a) in pale brown SEBs (e.g., Fig. 1c)	Barges are a new feature of the faded SEB; four more formed at progressively more westerly longitudes.
2009-Jul-20	High-opacity SEBZ observed at $4.8 \mu\text{m}$ (deep clouds) separating cloud-free SEBn and SEBs, visibly brown colour still present (Fig. 1c).	Zone-like conditions beginning at depth.
2009-Jul-24	Narrow lane of SEBZ higher opacity observed at $8.6\text{-}\mu\text{m}$ (upper clouds); SEBn and SEBs appear diffuse and cloud-free (Fig. 1c)	Aerosol opacity in new SEBZ appears different in $4.8 \mu\text{m}$ (deep clouds) and $8.6 \mu\text{m}$ (upper cloud) images.
2009-Aug-04	Fifth brown barge (B5) forms furthest west of the GRS	Circulation forming/revealing brown barges has propagated westward.
2009-Aug-06	Opacity of SEBs and SEBn equal at $8.6\text{-}\mu\text{m}$, but $4.8\text{-}\mu\text{m}$ opacity considerably higher over SEBs than SEBn; SEBs $8.6\text{-}\mu\text{m}$ opacity is higher west of the GRS than to the east (Fig. 2a); brown colour of SEBs fading west of GRS	SEBs fade west of GRS had begun.
2009-Oct	Brown colour of the SEBs east of the GRS begins to fade, bulk of the SEB acquired a pale orange tint.	Fade had progressed around the planet from its starting point west of the GRS.
2009-Oct-04	Brilliant white spot observed north of the GRS (Rogers, 2010a)	Uncertain connection to fade process
2009-Nov	All barges persist in faint red-brown southern SEB, only SEBn remains relatively cloud-free; SEBs has high cloud opacity at 4.8 and $8.6 \mu\text{m}$ and cannot be distinguished from SEB (Fig. 2a)	Fade has not yet completed, but cool SEBZ is fully established.
2010-Jan	End of 2009 apparition; SEBn narrow and dark; most of SEB pale orange; 5 barges dark and conspicuous	Fade had not yet completed.
2010-Apr	Start of 2010 apparition, all of SEB is pale, brown barges still faintly visible	SEB fade proceeded almost to completion while Jupiter was obscured by the Sun.
2010-Jul-01	SEBs is completely absent in $4.8\text{-}\mu\text{m}$ imaging, SEBn can still be seen (Fig. 2c). Visible images show brown barges have almost completely faded, but still partially outlined by faint blue-grey patches.	Deep cloud opacity completely covers SEB
2010-Jul-13	SEBs (narrow and undulating) and SEBn (broad) are detectable at $8.6 \mu\text{m}$, barges cannot be distinctly observed (except at $10.8 \mu\text{m}$, Fig. 5); central SEB covered by high opacity cloud (Fig. 2c)	SEB fade has completed.

Table 5: Characteristics of note during the SEB fade

Characteristic	Typical Latitude	Temporal Behaviour
GRS Wake	7-20°S	Filamentary turbulence normally dominates region NW of GRS (Fig. 1a-b; became quiescent in May-June 2009 (Fig. 1c); prelude to the formation of SEBZ and the fade.
SEBn	7-12°S	Dark, narrow brown lane separating SEB and EZ (Fig. 1a); warm cloud-free conditions persisted throughout fade; opacity increased but did not obscure 4.8 and 8.6- μ m emission completely (Fig. 2c).
SEBs	15-18°S	Broad dark band of variable width separating SEB and STrZ; began to fade west of GRS in June-July 2009; east of the GRS by October-November 2009. By July 2010 deep cloud opacity completely obscured SEBs 4.8- μ m emission; whereas a narrow lane of low upper-cloud opacity (8.6 μ m) was visible (Fig. 2c).
SEBZ	11-15°S	Cool zone-like temperatures developed July-August 2009 for $p > 300$ mbar and persisted to July 2010 (Fig. 5; Fig. 9); coincides with increased opacity of SEB centre and reduction of zonal windshear in upper troposphere (Fig. 6).
SEBs Undulations	17-19°S	Unique characteristic of fully-faded state in July 2010 (Fig. 2c); zonal oscillations of cloud opacity with 5-6° longitude wavelength and retrograde motion; further south than the typical SEBs edge.
SEBn Projections	6-9°S	Persistent features of SEBn, wave activity at the boundary between clouds of the EZ and SEB mixes cloud opacity. No change during the fade.
Brown Barges	14-16°S	Five dark brown barges in the SEBs (B1-B5) formed west of the GRS between June-August 2009 (as the SEBZ was forming, Fig. 2). All were cloud-free with warm core temperatures. Not observed in previous fades (Sanchez-Lavega and Gomez, 1996). Barges faded by July 2010, but warm cyclonic circulation was still present (Fig. 5).
GRS White Spot	9-11°S	White cloud (vigorous convective plume) near N edge of GRS in July 2010; high 8.6- μ m opacity (Fig. 10c), gives rise to a blue-grey streak northwest of the GRS (Rogers, 2010a). Uncertain connection to the fade process, but may have also been present during 1989-1993 fades (Rogers, 2010a).
SEBD	7-20°S	Expected vigorous convective disturbance that will signal the start of the SEB revival.

SEB Fade Sequence I: May 2008 - July 2009

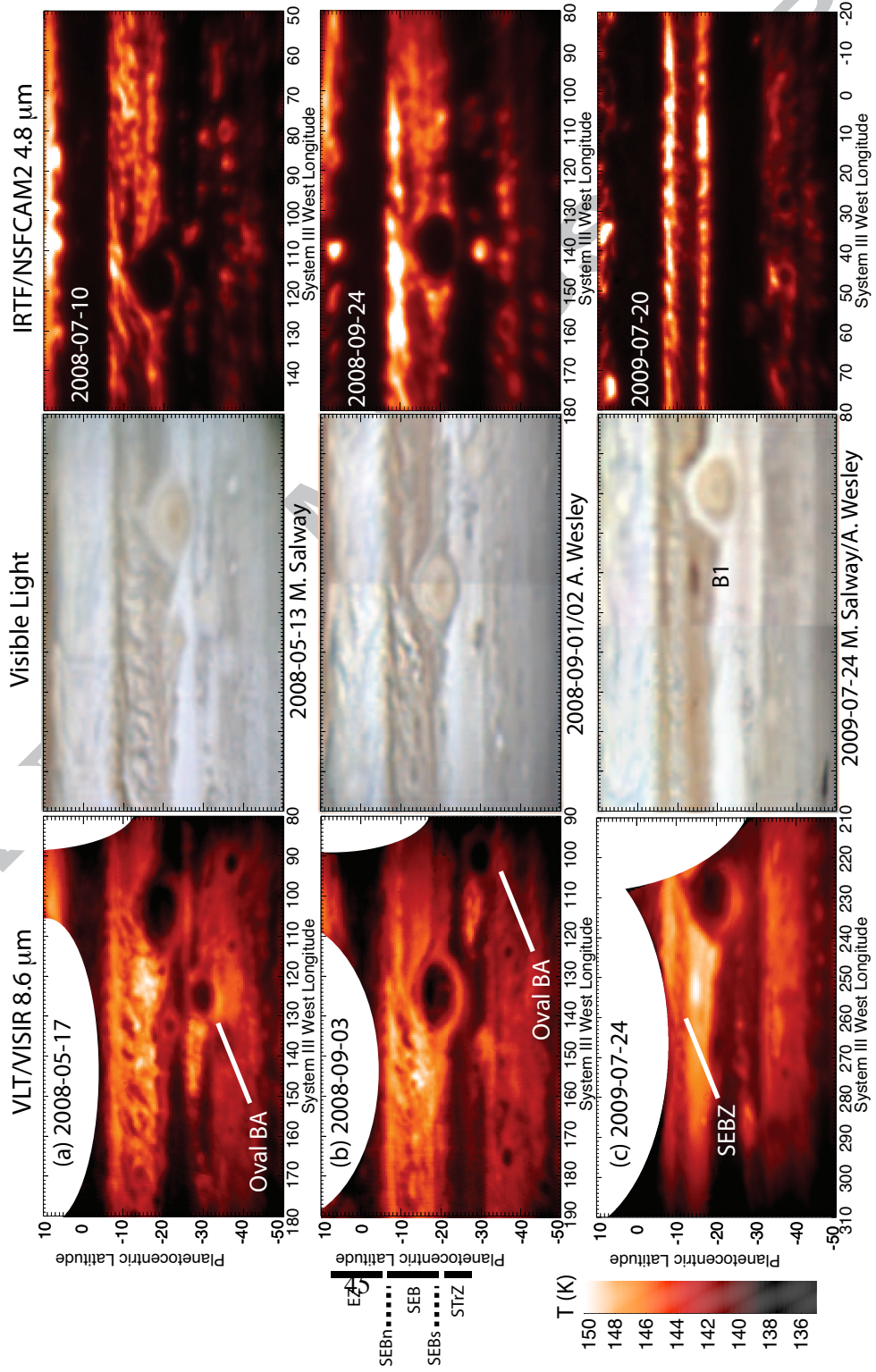


Figure 1:

SEB Fade Sequence II: August 2009-July 2010

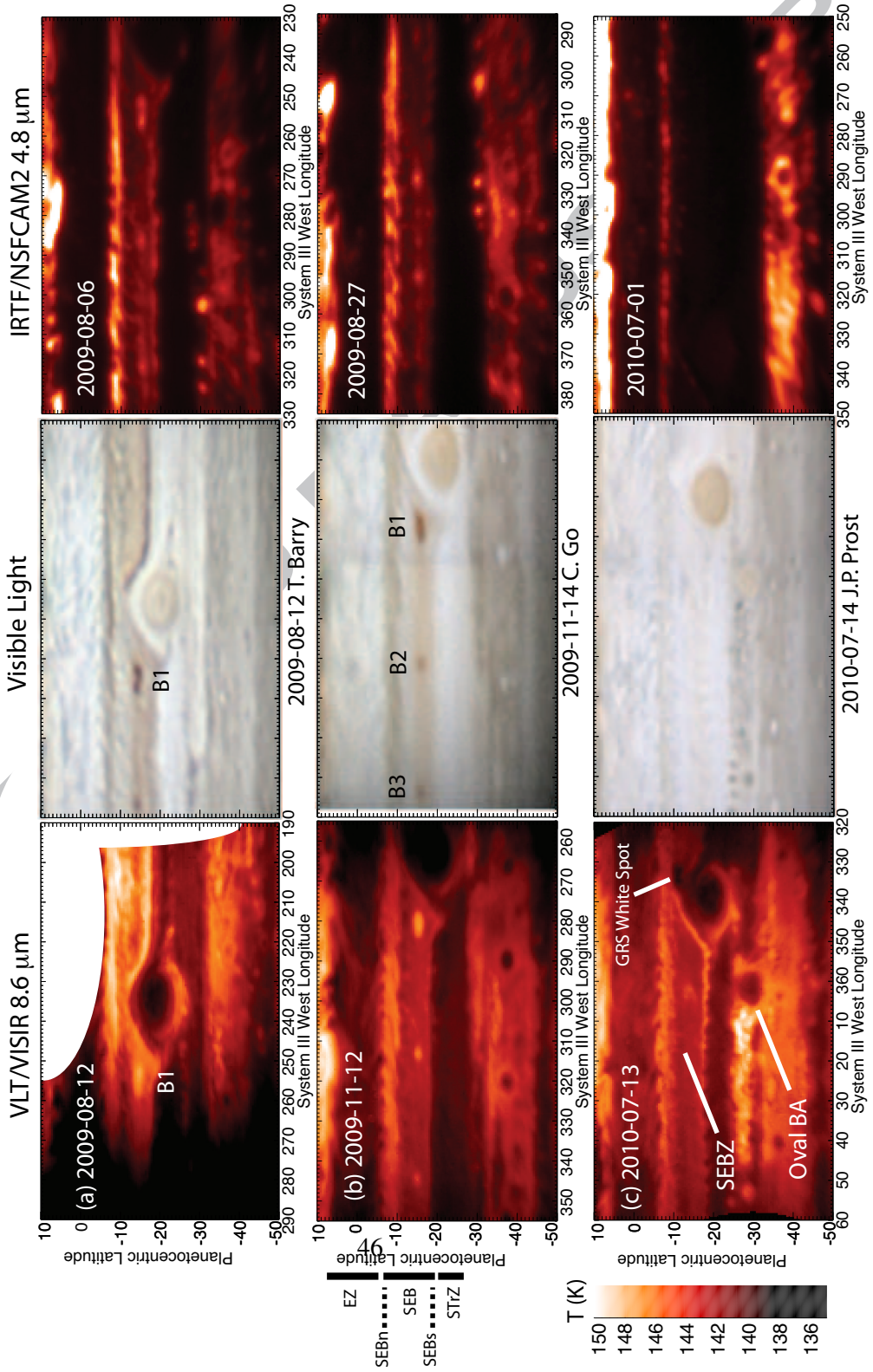


Figure 2:

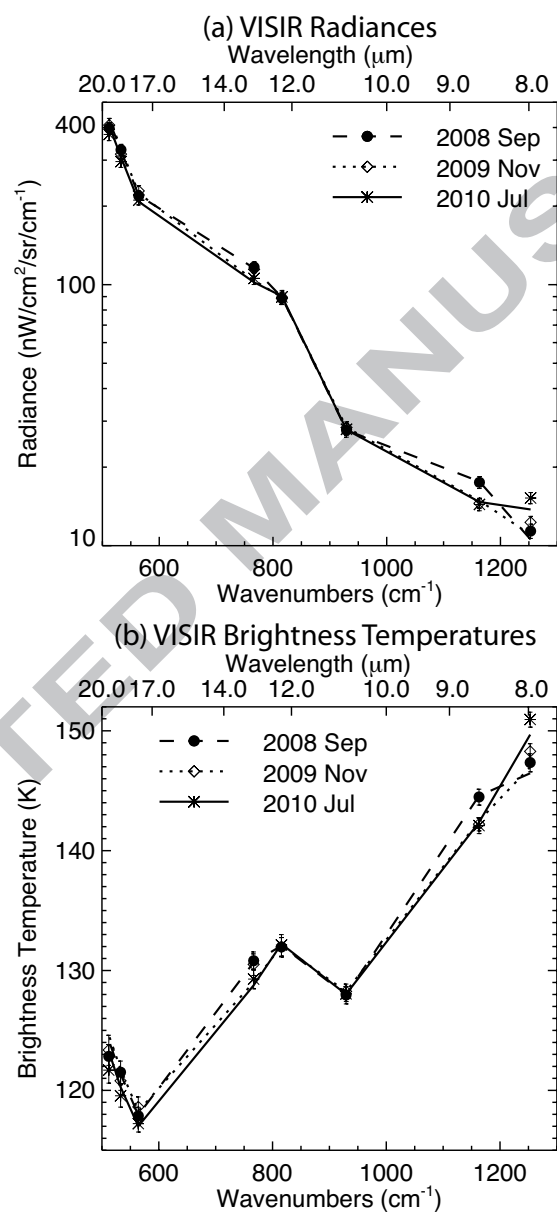


Figure 3:

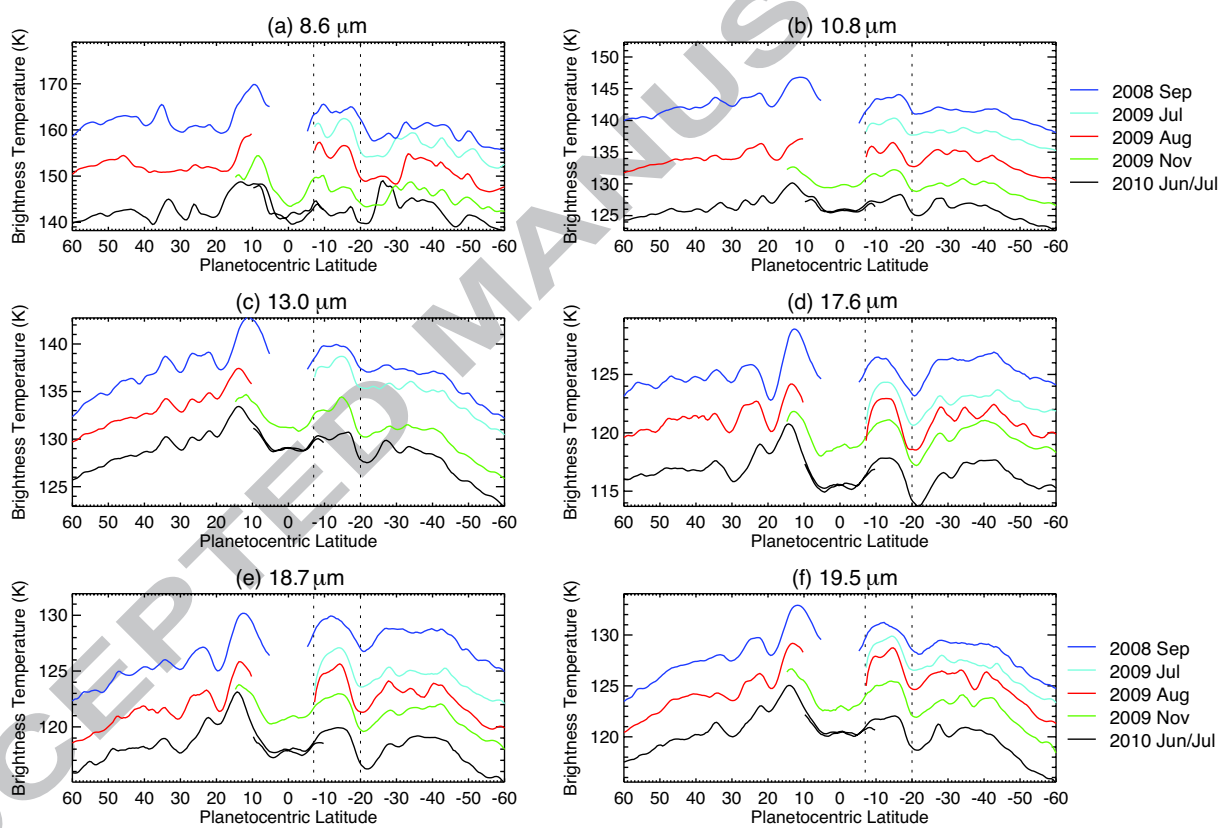
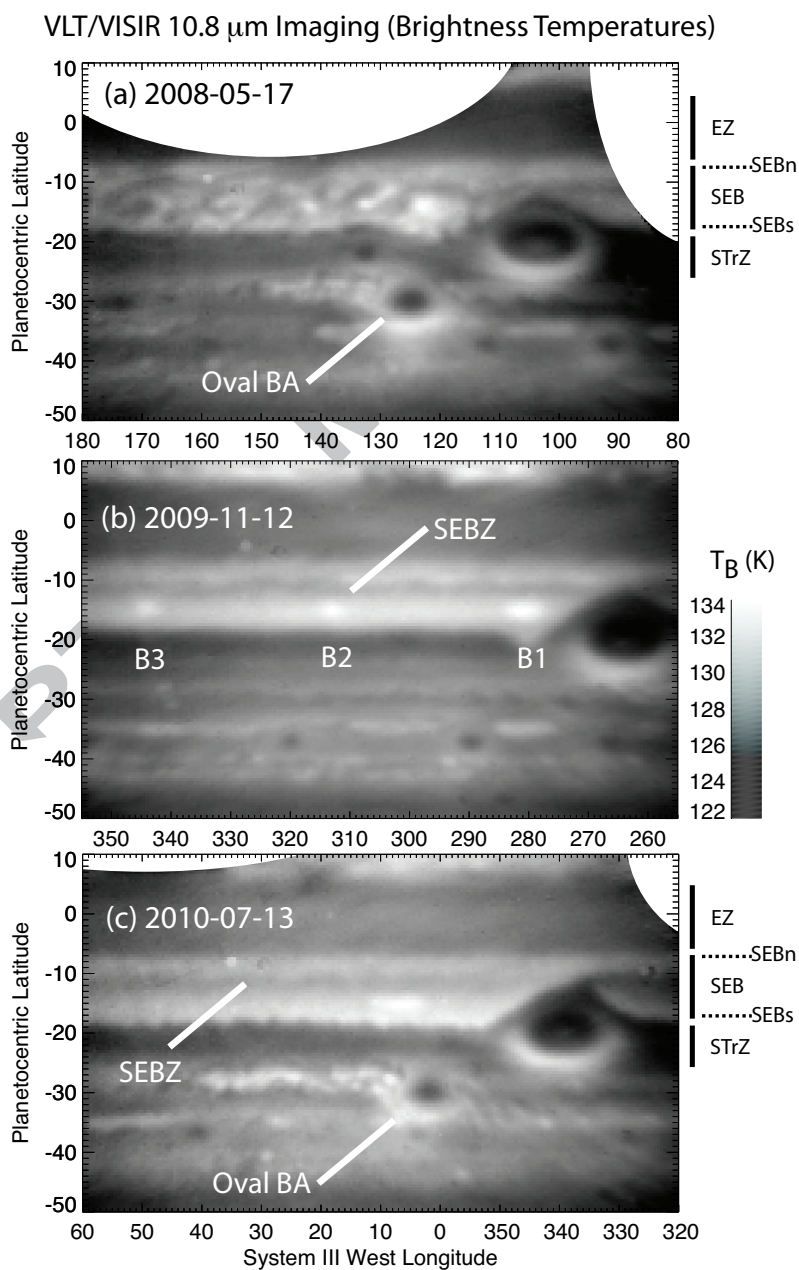


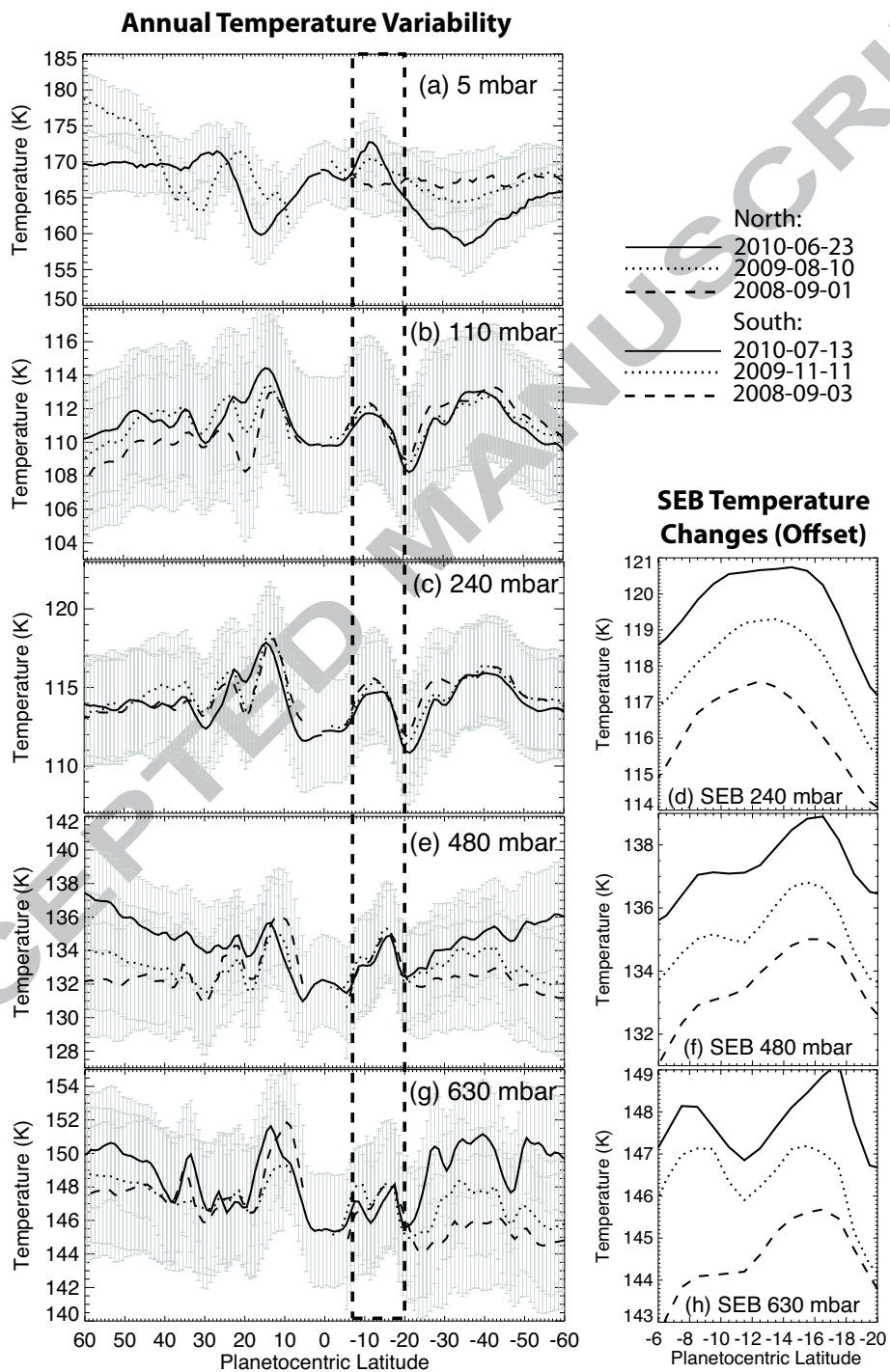
Figure 4:

IPT



49

Figure 5:



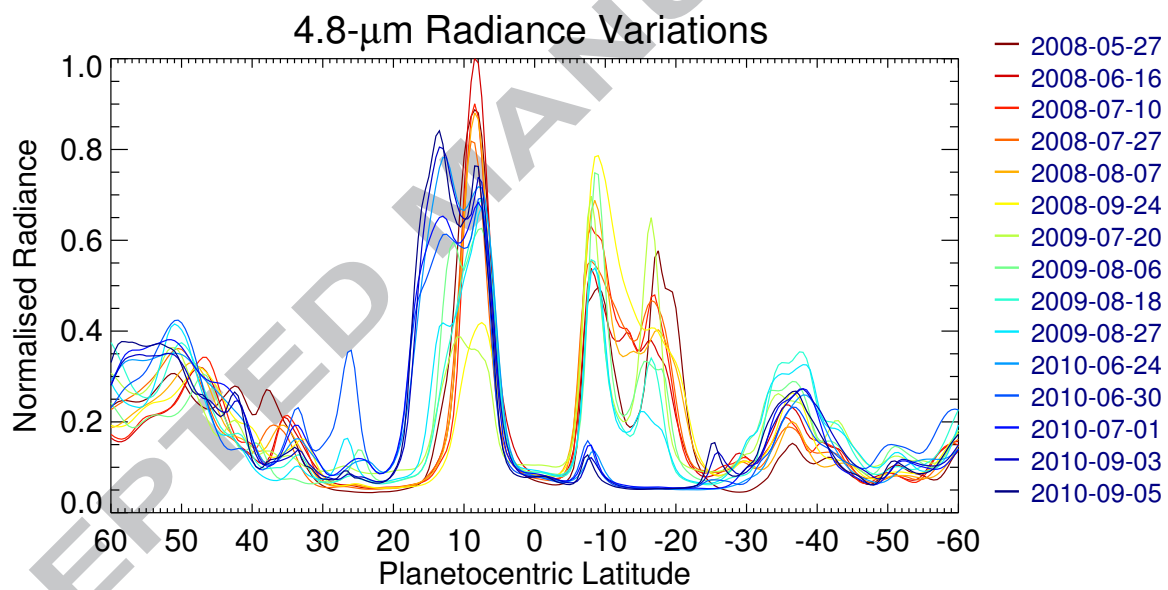


Figure 7:

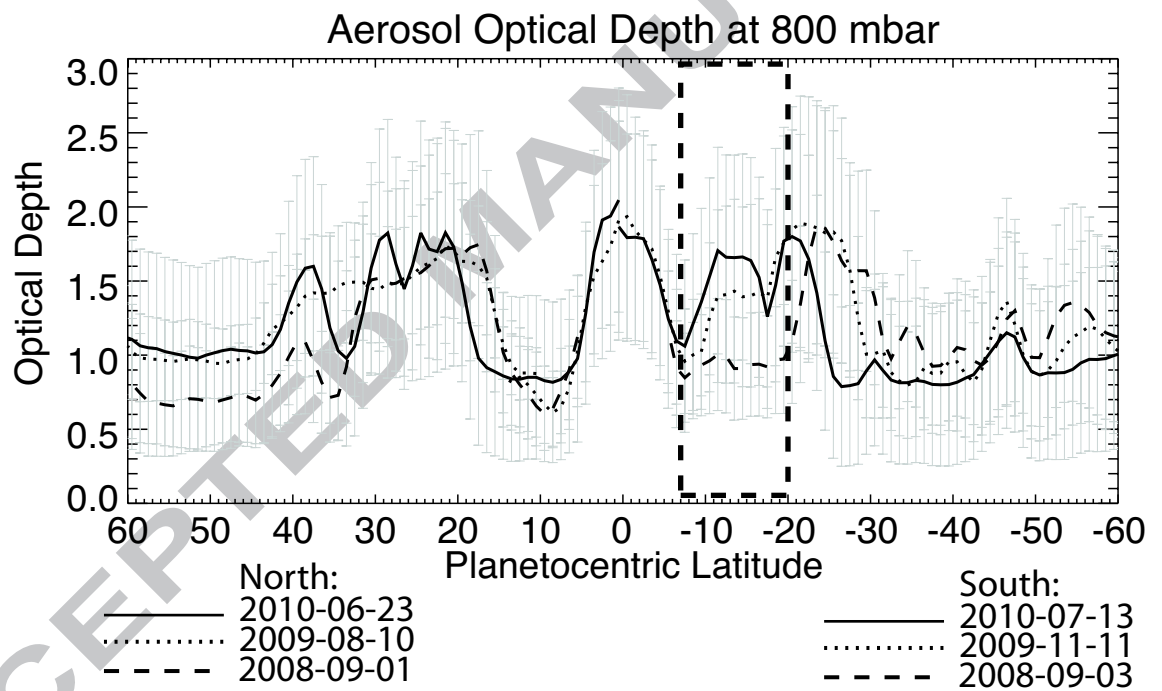


Figure 8:

ACCEPTED

RIPT

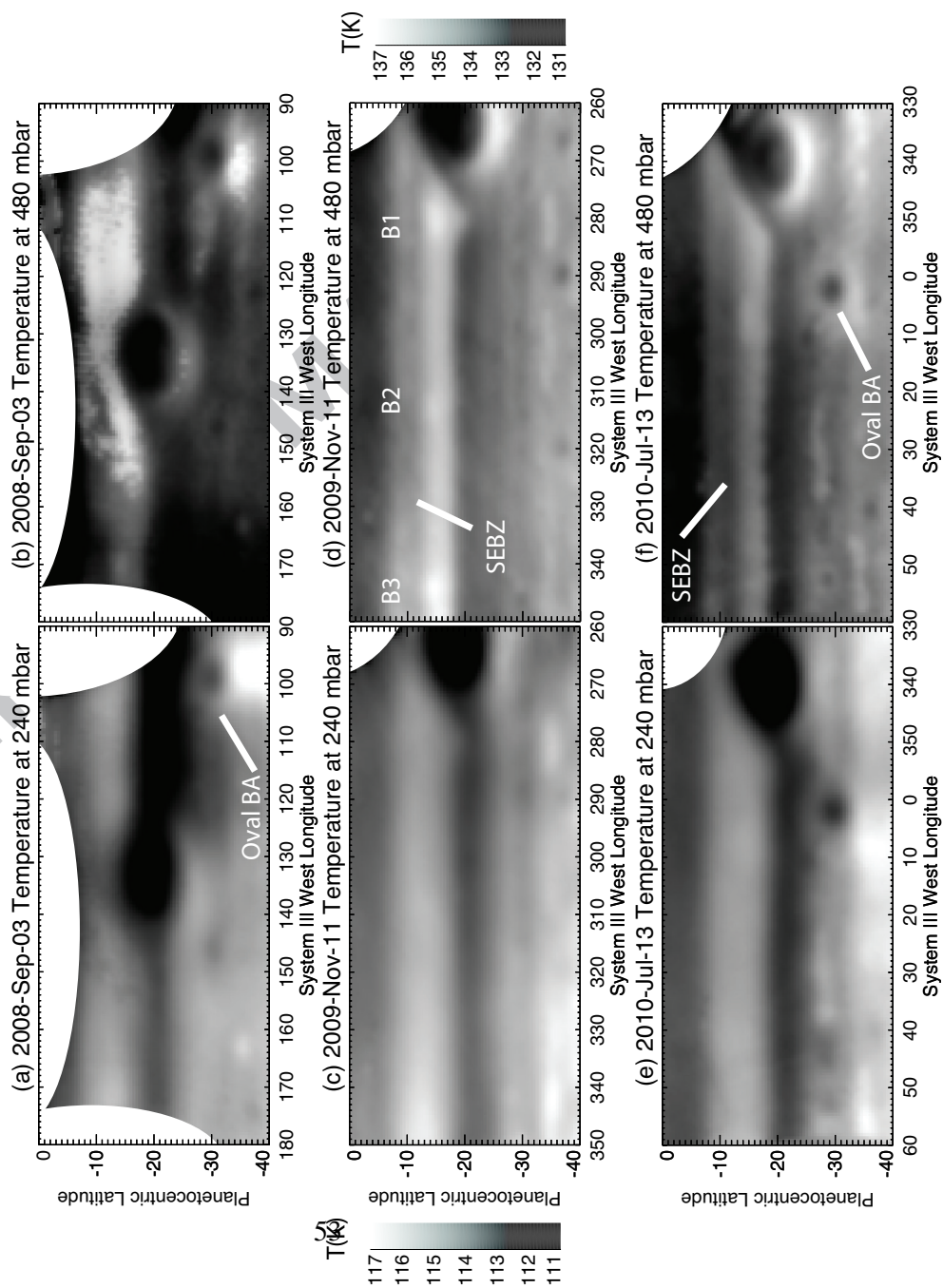


Figure 9:

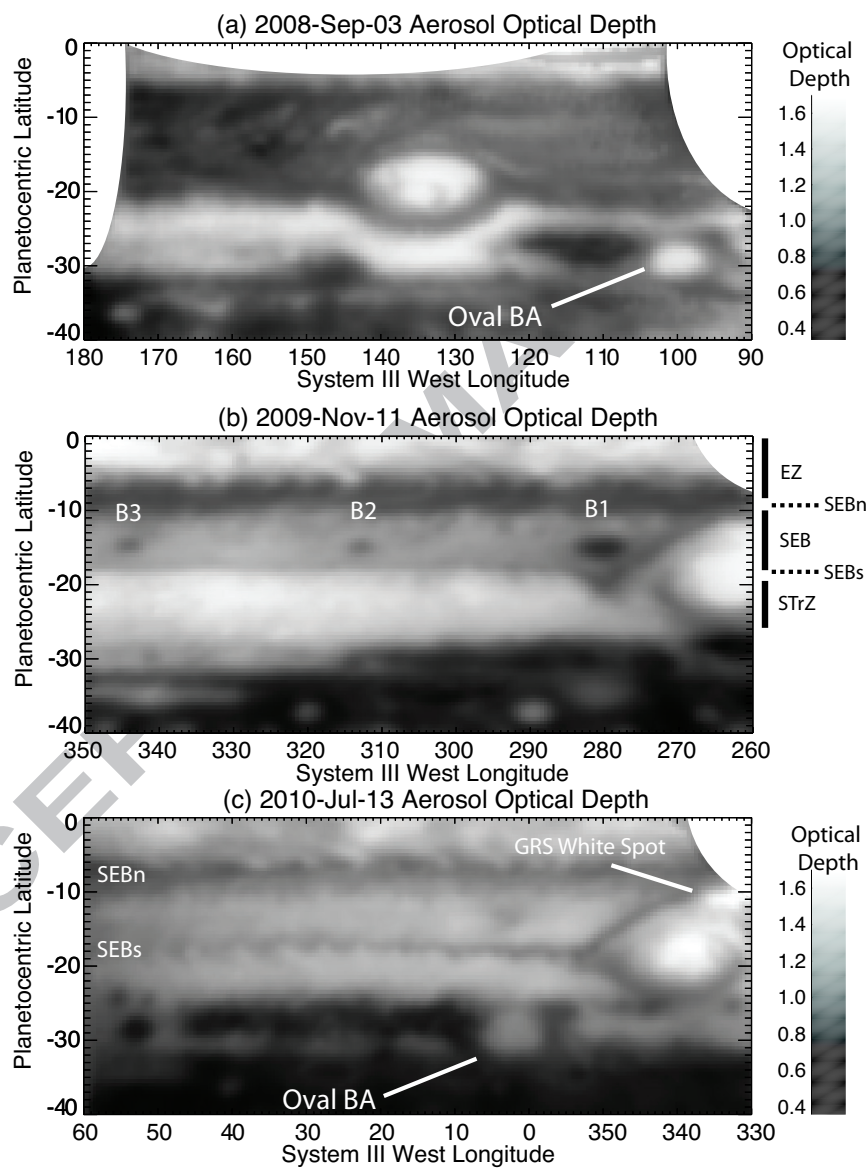


Figure 10:

898 **Appendix A. Phenomena at Other Latitudes**

899 The SEB life cycle is one of numerous dynamical phenomena evident in the
900 2008-2010 datasets, described briefly below. These events are not necessarily
901 connected to the SEB fade, but appear to be part of longer-term cycles or secular
902 changes (e.g., Rogers, 1995). We have chosen to include them for completeness.

- 903 • *Oval BA*: Oval BA is Jupiter's second largest anticyclone, which formed
904 from successive mergers and reddened in 2005 (e.g., Cheng et al., 2008).
905 The regular biennial passage of Oval BA past the Great Red Spot is evident
906 in Figs. 1-2. The cyclonic activity to the northwest of Oval BA, analogous
907 to the GRS wake, is considerably more elongated and brighter at $8.6 \mu\text{m}$ in
908 2010 than it was in 2008. This was the result of convergence with a large
909 cyclonic cell, which initiated a merger of Oval BA with a small anticyclonic
910 white oval and concurrent convective outbreak event in the cyclonic cell in
911 June 2010 (described in detail by Rogers, 2010b). This manifests itself as
912 clear cloud-free conditions in the cyclonic region to the northwest of the
913 oval in Fig. 10c, which also shows indications that Oval BA's aerosols were
914 less optically thick in 2010 than in 2008, although the oval remained red in
915 both years. Furthermore, the warm southern edge of Oval BA (Fig. 9) was
916 more diffuse and warmer in 2008, whereas it appeared offset to the west and
917 cooler by 2-3 K in 2010. It is unclear whether these changes are the result of
918 a weakening of Oval BA between 2008 and 2010, or simply due to different
919 environmental conditions in the STB surrounding the vortex.
- 920 • *Northern Equatorial Belt*: The visibly-dark brown NEB is the brightest
921 band on the planet at all thermal wavelengths (Fig. 11, 4). Despite being a

922 symmetric counterpart of the SEB, the NEB does not display the same clas-
923 sical fade and revival cycle. However, it does undergo occasional northward
924 broadenings that may be comparable events (Orton et al., 1994; Rogers,
925 1995), and have occurred every 3-5 years since 1988. The latest such event
926 occurred between in 2009: the NEB expanded northwards from 15°N to
927 18°N, at visible and thermal wavelengths, causing a narrowing of the ad-
928 jacent cool North Tropical Zone (NTrZ). This expansion corresponds to a
929 clearing of aerosol opacity between 15-18°N between 2008 and 2010 (Fig.
930 7, Fig. 8), as well as a warming of 3-4 K in the upper troposphere for the
931 NEBn (Fig. 6). Orton et al. (1994) also noted warming associated with
932 an earlier NEB expansion. The resulting decrease in dT/dy between 15 and
933 20°N means that the prograde jet at 21°N is subject to smaller vertical wind-
934 shear and can persist to higher altitudes in the stratosphere. Finally, the NEB
935 demonstrates dramatic longitudinal wave activity with a 25-30°wavelength
936 in 2009 (Fig. 11(b)), which was not apparent in the SEB at any time during
937 2008-2010. The thermal waves may be associated with an alternating array
938 of anticyclonic and cyclonic ovals observed in visible light, some of which
939 were newly formed as part of the expansion event (Rogers, 2010a; Rogers
940 et al., 2004).

- 941 • *Northern Vortices:* Large red anticyclones also occur in the northern hemi-
942 sphere at 38°N in the North North Temperate Zone (NNTZ). The largest of
943 these, named NN-LRS-1, is frequently reddish; almost as large as Oval BA;
944 and has existed at least since 1993 (Rogers et al., 2011). It is prominent as
945 a dark oval at thermal wavelengths in Fig. 11a, and appears larger at 8.6
946 μm than it does at 10.8 μm , suggesting that the region of elevated aerosol

947 opacity extends over a wider area than the cold temperature conditions at
948 the centre of the storms. This is similar to the observed properties of Oval
949 BA itself in Figs. 1-5.

950 • *North Temperate Belt:* Besides the SEB, the warm NTB (21-28°N) is one
951 of the most active regions on the planet, also demonstrating sporadic fade
952 and revival cycles. The last such revival of the faded NTB occurred in
953 2007, with the appearance of two high-altitude plumes with wakes of tur-
954 bulent dark brown material rapidly encircling the planet (Sánchez-Lavega
955 et al., 2008; Rogers, 2007a). The revival resulted in a broad red NTB with
956 a component of high-altitude tropospheric haze (200-400 mbar) detectable
957 in methane-band imaging at 2.3 μm (Sánchez-Lavega et al., 2008). Accord-
958 ingly, the NTB has remained dark at 8.6 μm between 2008 and 2010 (Fig.
959 11), indicating the continued presence of high aerosol opacity similar to the
960 EZ and the faded SEB (Fig. 8) and making it almost as dark as the cold
961 NTrZ (18-21°N). The exceptions to this rule are discrete cloud-free barges
962 of high 8.6- μm flux, which are the darkest parts of the revived NTBn in vis-
963 ible light and probably coincide with features of high 4.8- μm flux (although
964 IRTF/NSFCAM2 and VLT/VISIR did not observe simultaneously).

Research Highlights**Fletcher et al.***Jovian Temperature and Cloud Variability during the 2009-2010 Fade of the South Equatorial Belt*

1. The 2009-10 whitening of Jupiter's SEB was the first complete SEB life cycle since 1992-1993.
2. Upwelling increased the infrared opacity of the SEB several months before the whitening.
3. A cool zone-like region formed in Jupiter's convective troposphere before the visible fade began.
4. Enhanced ice condensation likely caused the dramatic clouding over of the SEB.
5. The revival required sublimation of these ices to reveal the belts typical brown colours.